Delft University of Technology

MSC THESIS
BM51032

Do the elderly use thigh push off in sit-to-stand to compensate for a lack of stability?

Application of the Stability Basin method to assess the stability of compensatory sit-to-stand strategies in young and elderly participants

Janna Worp (4233948)
MSc Biomedical Engineering TU Delft

Supervisors:
Dr.ir. Eline van der Kruk (Biomechanical Engineering TU Delft)
Dr.ir. Sjoerd Bruijn (Human Movement Science VU Amsterdam)
Prof.dr.ir. Jaap Harlaar (Biomechanical Engineering TU Delft)
June, 2021

Abstract

Background Due to neuromuscular capacity decline, sit-to-stand, an essential daily life activity, is increasingly difficult to perform for elderly. In practice, elderly frequently use compensatory arm-strategies in sit-to-stand. However, the specific advantages of these compensatory strategies are unclear. **Aim** The focus of this research is to study the influence of thigh push-off, a common compensatory strategy, on the stability of sit-to-stand for both the young and elderly. **Method** Motion data was retrieved from 50 young and elderly participants who performed sit-to-stand with and without thigh push-off. To mimic realistic daily-life strategies, participants were not restricted in sit-to-stand style in any way but arm-use. The experimental sit-to-stand data was fitted to a pendulum model with feedforward and feedback control to simulate the stability limits of the observed sit-to-stand strategies. The model allows us to explore stability limits without the need of perturbation. For each arm-strategy and participant a stability basin, i.e. all potential trajectories of motion, was formed. We compared the stability basins between arm-strategies and between age-groups. **Results** The size of the computed stability basin for thigh push-off was larger than for no arm push-off implicating thigh push-off is a more stable sit-to-stand strategy. The difference between arm strategies was larger for the elderly than for the young participants. Overall, the stability basins of the elderly were larger compared to those of the young participants, for both arm strategies. **Conclusion** The resulting stability basins suggest that thigh push-off increases the stability of sit-to-stand and thus could indeed be an effective compensatory strategy. Stability basin shape differences indicate that without thigh push-off elderly compensate for possible early sit-down and a step halfway sit-to-stand, and with the thigh push-off strategy only for early sit-down. The age-groups differences confirm stability basins quantify the stability of the observed movement strategy rather than the stability of the participants. We observed that elderly use more precautious sit-tot-stand movements.

1 Introduction

The ageing of the world's population goes hand-in-hand with a growing number of people that cope with mobility impairments. Limited mobility (due to age-related capacity decline) increases the likelihood of falling. At present, the consequences of older adult falls and it's treatment are increasingly straining the health care system.[1] Moreover, mobility impairments limit independency and decrease quality of life. Research to better understand mobility impairments is crucial for the development of preventative care which in turn reduces health care costs and increases older age life quality.

An important daily-life activity that becomes increasingly difficult for elderly is sit-to-stand. It is a crucial transfer movement with a large influence on a person's independence. In biomechanical terms it can be described as an aperiodic movement where the centre-of-mass (COM) is translated horizontally and vertically from a stable to a less stable position.[2] In practice, elderly frequently use compensatory arm strategies such as pushing off on the thighs or using arm rests.[3] It has been hypothesized that elderly use these compensatory strategies to increase stability, compensating for their increased risk or fear of falling and/or reduced lower limb muscle strength. However, current sit-to-stand stability research has been limited to restricted sit-to-stand strategies without arm-compensation. Furthermore, stability is difficult to quantify, especially in aperiodic unrestricted movements, without using perturbations.[4]

The aim of this study is to research if thigh push-off (TH) increases stability of sit-to-stand compared to when no arms (N) are used in realistic, natural sit-to-stand. In the experiment, elderly and young participants performed self-preferred sit-to-stand movements for the two separate strategies. To assess the stability of the two strategies we used the stability basin method. Stability basins explore the limits of an observed movement strategy without perturbations. The method fits an individual-specific pendulum model with feedforward and feedback control to a set of strategy-specific sit-to-stand observations and then uses simulations to find the limits of the observed strategy. All simulated possible trajectories that reach standing successfully, *without a change of strategy*, together form the stability basin. A larger computed stability basin indicates a more stable observed movement strategy, providing an overall metric of stability. Stability basins can be computed for any sit-to-stand strategy enabling studying unrestricted strategies. Furthermore, stability basins enable studying stability throughout the movement enabling identification of momentary differences in stability next to providing quantification of overall stability of the observed movements.[5]

In the development of the stability basin method, Shia et al.[5] proved stability basins can indicate distinct differences in stability between two restricted sit-to-stand strategies (using momentum or exaggerated trunk flexion) for healthy young participants. In a follow up study, Holmes et al. [6] validated the predictive power of the stability basin when compared to actual sit-to-stand observations perturbed to failure (sit or step). For different feedback and feedforward controller models, stability basins were robust in predicting successful trials (±98% correct success prediction) but varying in predicting unsuccessful trials correctly (23.0-85.0% correct failure prediction) depended on controller model. Both studies recommended the use of stability basins in longitudinal studies to assess the stability of an individual with regards to e.g. ageing or rehabilitation. In our study, we will be the first to 1) apply the method to unrestricted sit-to-stand strategies and 2) apply the method on sit-to-stand observations of elderly participants.

We hypothesised that 1) the stability basins for thigh push-off are larger than that of sit-to-stand without arms, indicating thigh push-off is a more stable strategy, and 2) the stability basins of the older adults are smaller than that of young adults as we assume that the elderly have a higher risk of falling and thus are more unstable.

2 Method

To determine whether the thigh push-off (TH) is more stable than the no arms strategy (N), we estimated stability using the stability basin method with experimental data from young and older adults[3].

The main steps in the computataion of a stability basin are illustrated as red boxes in figure 1. The stability basin method fits a pendulum model with feedforward and feedback control to observed data. With the fitted sit-to-stand model the limits of the observed strategy are explored via simulation. All successful simulated trajectories together form the stability basin describing the stability of the arm-strategy of the participant.

The simulative model with which we compute the stability basin can be described in three parts as illustrated in the purple sub boxes in figure 1. First, the equations of motion that are effective for the pendulum model. Second, the modelled input, modelling the acting forces on the system, defined by feedforward and feedback control. Thirdly, a target set defining what is successful standing, which acts as the set of initial points for the simulation. These three parts are fitted and optimised such that the model represents the observed sit-to-stand strategy. The observed, full-body motion sit-to-stand data is processed in several steps to comparable centre-of-mass trajectories such that they fit the sit-to-stand model.

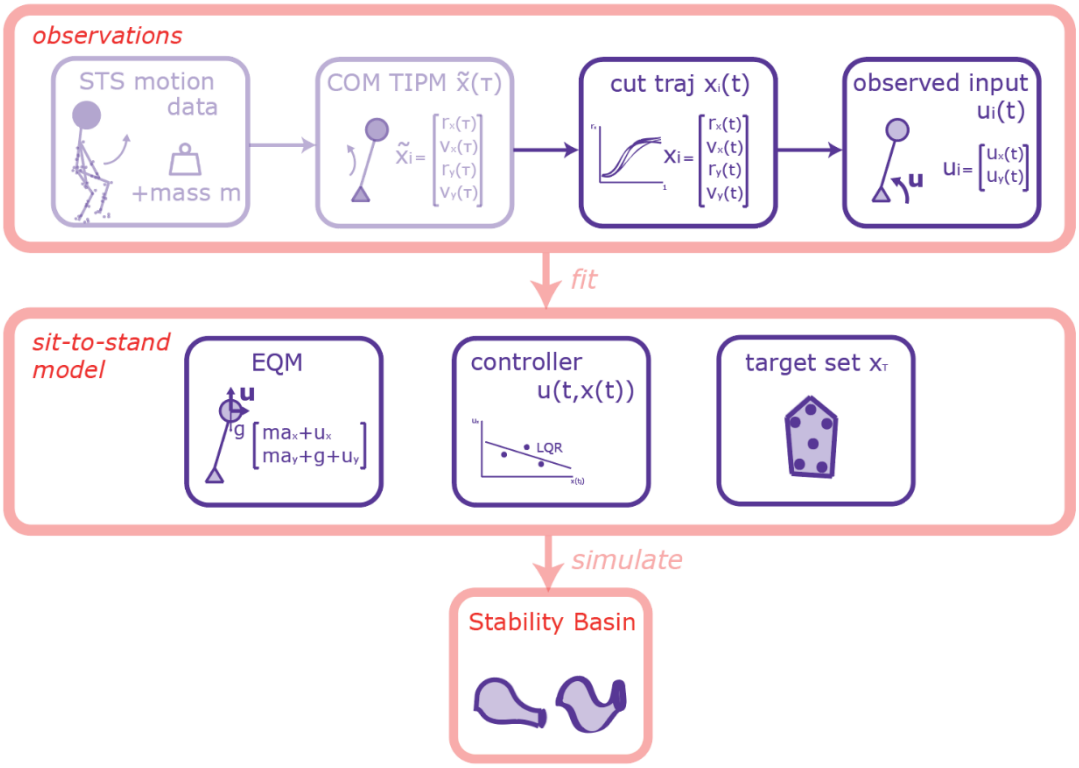

Figure 1 Block Scheme Stability Basin method. The red boces indicate the main steps of the method. A sit-to-stand model is fit to observed data and with that model we simulate the limits of the observed sit-to-stand movements, expressed as a stability basin. The purple boxes indicate substeps in the method. The sit-to-stand observations are reduced to centre of mass trajectories to fit a telescopic inverted pendulum model (TIPM), the trajectories are cut and normalised and observed input is modelled using inverse dynamics. The sit-to-stand dynamics are described by equations of motion (EQM), input described by a controller and what is successful standing by a target set. The stability basin is the result of a backward reachability analysis of the sit-to-stand model.

2.1 Sit-to-stand model

We computed the possible sit-to-stand trajectories, forming the stability basin, with simulation of a sit-to-stand model. We modelled the participants as an inverted pendulum and the observed sit-to-stand strategy as a controller. Finally, for simulation, we derived a definition for what is successful standing; the target set.

2.1.1 Telescopic inverted pendulum model

The observed centre-of-mass trajectories were further simplified using a simple model: a telescopic inverted pendulum model (TIPM). A TIPM comprises of a single mass with a position relative to a base. The mass of the pendulum was the participant's measured mass. The base's forward positon was identical to the anterior-posterior ankle position, the height was set at ground level. This base approached the centre-of-pressure without the use of a force plate. Medio-lateral movement is neglected; the TIPM only describes the dynamics in the sagittal plane. Using the TIPM enabled us to reduce dimensions. We neglected medio-lateral balance and translated each observed trajectory to the same point, relative to the base, such that all observed trials could be aligned and compared.

We describe the anterior-posterior, forward or horizontal direction as the x-direction, the upward direction or transversal axis as the y-direction. Hereafter, these directions are denoted as subscripts. The TIPM describes the position and velocity in a state trajectory **x(t)** with four state components. The position of the pendulum's mass, relative to base, notes as $\mathbf{r_x}$ and $\mathbf{r_y}$. We denote the velocity components as $\mathbf{v_x}$ and $\mathbf{v_y}$.

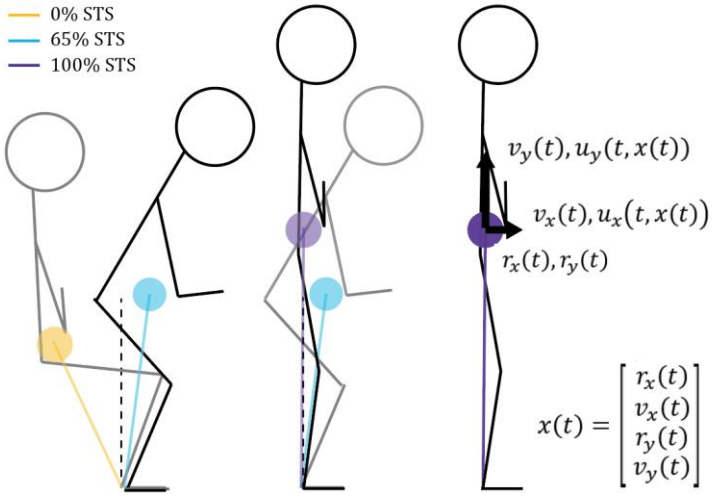

Figure 1 Telescopic Inverted Pendulum Model: describes full-body centre-of-mass trajectories relative to a base as a four-variable state vector neglecting medio-lateral displacement.

Equation of Motion

In the dynamic model we neglected angular momentum. External forces are gravity, gravitational force set at g = 9.81 m/s^2, and the input force **u** produced by the subject. The real-life muscle input of the participant is modelled as a single input force vector with a horizontal and vertical component. The input force **u** is modelled by the controller **u(t,x(t))** which is time and space dependent due to the feedback and feedforward control.

$$\begin{bmatrix} \sum F_x \\ \sum F_y \end{bmatrix} = \begin{bmatrix} m * a_x + u_x \\ m * a_y + m * g + u_y \end{bmatrix} \quad (1)$$

2.1.2 Model input: controller

The controller models the input **u(t,x(t))** the participant used during sit-to-stand. It has a feedforward, or predictive (dependent on time) component. And, a feedback, or reactive (dependent on space), component[5]. The feedback control accounts for the ability to adapt to small perturbations[7,8]. When a perturbation is too large for the feedback control to handle, the subject must switch to a new controller to achieve the original task which involves changing the feedforward component[9]. Both the feedforward and feedback component were fitted on the observed data such that it modelled the subject's strategy-specific behaviour. Therefore, the controller was fitted separately for the different instructed arm-strategies (no arm use, thigh push-off).

LQR controller

The Linear Quadratic Regulator (LQR) controller is based on proportional-derivative feedback about the average trajectory of the observed trials, hereafter called the *average nominal trajectory* $\mathbf{x_{nom}}$, to correct for deviations[5]. The feedforward control is the direct input from the average nominal trajectory; $\mathbf{u_{nom}}$, derived using inverse dynamics with the equation of motion of the pendulum. (*eq1*).

$$u\big(t,x(t)\big) = u_{nom} + u_{fb}(t,x)$$

$$u\big(t,x(t)\big) = u_{nom} + K(x(t) - x_{nom}(t))$$

Feedback gain **K**[2x4] was determined by minimising the quadratic cost of the input determined by the controller **u(t,x$_i$(t))** and the estimated observed input $\mathbf{u_i}$ over each observed trajectory **i**. Gain **K** is generated from optimised state weight matrix **Q** [4x4] and input weight matrix **R** [2x4] (*eq2*)[10]**.** The time vector was discretised in 200 time steps such that t = [0,1] and dt = 0.005:

$$min \sum_i \int_0^1 \big(u\big(t,x_i(t)\big) - u_i(t) \big)^2 dt \qquad (2)$$

$$\min_{Q,R} \sum_i \int_0^1 \begin{Bmatrix} \overline{\mathrm{X}}^T * \mathrm{Q} * \overline{\mathrm{X}} + \\ u_{fb}(t)^T * R * u_{fb}(t) \end{Bmatrix} dt \quad \text{with} \quad \overline{\mathrm{X}} = (x(t) - x_i(t))$$

Equation 2 Optimisation of the state and input weight matrices to optimise the controller to the observed data

In optimisation, Q was constrained to Q | {$Q_{i,j}$ = 0 V i=j: $Q_{1,1}$ = [$1e^{-5}$ $1e^{-2}$], $Q_{2,2}$ = [$1e^{-6}$ $1e^{-1}$], $Q_{3,3}$ = [0.1 100], $Q_{4,4}$ = [0.1 100]} and R was constrained to R | { $R_{i,j}$ = 0 V i=j: $R_{1,1}$ = [$1e^{-5}$ $1e^{-2}$], $R_{2,2}$ = [$1e^{-6}$ $1e^{-1}$]}. Relative costs were restrained such that no input could cost ten times more than any other input and no state could cost more than 100 times any other state.

2.1.3 Target Set

The stability basin shows the possible trajectories which end in successful standing without change of controller. What is 'successful standing' was defined by the target set. The target set was, just like the controller, fitted to the observed trajectories. We created the target set by forming a convex hull around the end points (100% sit-to-stand) of the observed trajectories. Our state trajectory has four dimensions ($\mathbf{r_x}$, $\mathbf{v_x}$, $\mathbf{r_y}$, $\mathbf{v_y}$). In order to compute a convex hull in four dimensions, we needed at least five points. However, we had three observed trajectories and thus three points. Therefore, to compute the target set ($\mathbf{x_T}$), we modelled an 'extra point' for each measured end point. Figure 3 visually presents this computation. The extra points were generated to be very close to the measured points so that the fabricated target set approached the actual target set.

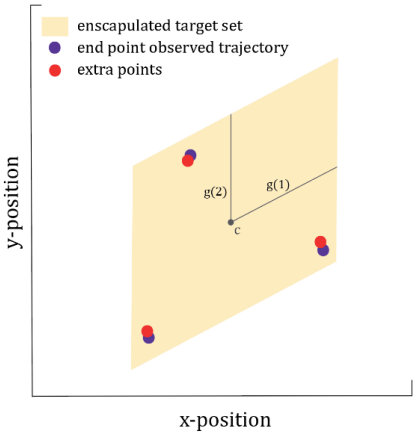

Figure 2 Target Set zonotope computation in two dimensions. Note that, for two dimensions, we need at least three points to form a convex plane.

$$x_T = \begin{bmatrix} r_{x1}(1) & \cdots & v_{y1}(1) \\ \vdots & \ddots & \vdots \\ r_{x3}(1) - 0.001 * R & \cdots & v_{y3}(1) - 0.001 * R \end{bmatrix} [4x6]$$

Where **R** is a random number between 0 and 1.

To save computational time, the target set was saved as a geometric object called a zonotope, as demonstrated by Holmes[6]. A zonotope is defined by closed linear maps in *n* dimensions, four in our study, each for every component of state trajectory *x(t)*. Each map is parametrised by a centre c and g(1)-g(p) generators.[11] The use of zonotopes was automated applying the open-source reachability toolbox CORA in MATLAB. This toolbox was applied again in simulation with the stability basin computation.

Each generator was expanded by 20% conform recommendations [6] to avoid excluding observed states laying on the edge of the target set.

2.2 Stability basin computation: backward reachability analysis

With simulation of the fitted sit-to-stand model we explored the limits of the observed sit-to-stand strategy. All trajectories found in simulation that reach successful standing, as defined by the target set, together formed the stability basin.

The simulation uses simple numerical integration. As described earlier, the pendulum model dictated the equations of motion of the system *(eq1)* and the controller the input forces of the participant. For numerical integration, we further require an initial position. However, we are interested in a set of positions: all positions that lie within the target set. Therefore, we used reachability analysis. This method allowed the simulation of a set of points simultaneously, defined in a zonotope, using the CORA toolbox. As we simulated backwards from the target set, we computed the backwards reachable set to form the stability basin.[6]

Each stability basin was formed from 200 zonotopes so that the time vector is [0,1] with a unitless time step $\Delta t = 0.005$ [-]. Each zonotope spanned four dimensions ($\mathbf{r_x}$, $\mathbf{v_x}$, $\mathbf{r_y}$, $\mathbf{v_y}$) resulting in a four-dimensional stability basin. To save computation time, the maximum number of generators describing the zonotope was set to 800 generators[6].

2.3 Sit-to-stand data pre-processing

To fit the pendulum model we converted the observed full-body sit-to-stand kinematics to centre of mass (COM) trajectories. The observed COM trajectories were cut and normalised so that we could, from trials with different lengths, compute the stability basin from 0 to 100% sit-to-stand. Finally, we derived the observed input $\mathbf{u_i}$ directly from inverse dynamics which was used to optimise the controller input (section 2.1.2).

2.3.1 Anthropometric model

For a full description on the calculation of the segment COM location, the segment lengths, segment anatomical coordination systems (ACSs), body segmental parameters (BSPs) and circumference approximation we refer to appendix B.

From the captured marker data, we modelled the participant's movement using a 14 segment rigid body model: feet, calves, thighs, pelvis, abdomen, thorax and upper arms are separate segments directly modelled from marker positions. We neglected the hand position or wrist flexion by combining the forearm and hand to one segment where the position is solely based on forearm markers. The head's location was an approximation based on extrapolation of the thorax and assumed the head was aligned to the thorax.

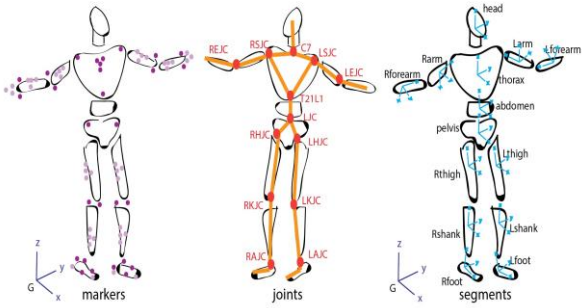

Figure 3 Anthropomorphic model concept. The segment and joint positions are estimated from the marker data. Body segmental parameters are obtained with approximated circumferences.

The variety of subjects, both in age and gender, attended careful consideration of method choice to model body segmental parameters (BSPs). Studies showed that 51% of the variability in BSPs is accounted for by body mass index (BMI) where age accounts for an additional 3-19%[12]. Considering one should choose an anthropomorphic model based on a subject group similar to one's study group [13], we applied a model based on adjustments to Zatsiorksy by de Leva[14] on the young participants, and a model developed for older adults by Pavol[15] on the elderly participants.

Unknown circumferential data was approximated based on measured BMI values and correlations from BMI related studies or assumptions based on a standard UK size chart (Belstaff Men's sizing Chart, 2020)]. Navel height was deducted from participant photos taken during the experiment.

The estimated total mass was modelled with a maximum difference of 10% to the measured mass for 42 participants, including 22 participants with a maximum difference of 5%. The six participants with a larger difference were mainly older men. All body segmental parameters are scaled linearly with the same factor such that the sum of the masses of the body segments corresponds with the measured total body mass. The differences in the anthropometric model with reality are expected to have a maximum effect on the height of the total body centre-of-mass of 5 cm.

We deducted the total body centre of mass throughout the movement combining the body segments' locations.

2.3.2 Trial segmentation and trial normalisation

To compare trials independent of their difference in duration, we normalised each state trajectory $\mathbf{x(\tau)}$ over the trial's length T such that we obtained unitless time interval $\mathbf{t}$ = [0,1][-], or 0 to 100% sit-to-stand, from the original time interval $\boldsymbol{\tau}$ [s].

$$\tau = [0, T]\ [s] \rightarrow t = \frac{\tau}{T} = [0,1]\ [-]$$

$$\tilde{x}(\tau) = \left[\widetilde{r_x}(\tau)\ \ \widetilde{v_x}(\tau)\ \ \widetilde{r_y}(\tau)\ \ \widetilde{v_y}(\tau)\right]'$$

We obtained the normalised state trajectory x(t) by scaling the velocity components with trial length T. Forces and accelerations were scaled with T^2 following the same logic.

$$x(t) = [\widetilde{r_x}(T * t)\ \ T * \widetilde{v_x}(T * t)\ \ \widetilde{r_y}(T * t)\ \ T * \widetilde{v_y}(T * t)]'$$

$$x(t) = \left[r_x(t)\ \ v_x(t)\ \ r_y(t)\ \ v_y(t)\right]'$$

Before normalisation, the trials had to be aligned and cut such that they resemble the most alike shape. We achieved this using an iterative process which used a scaled version of the average nominal trajectory $\mathbf{x_{nom}}$. This process is described in full detail in appendix C.

The start of the trial ($\tau = 0$, $t = 0$) was defined as when the horizontal acceleration first reached 15% of the peak horizontal acceleration of the aligned best scaled $\mathbf{x}_{nom}$. The end of the trial ($\tau = T$, $t = 1$) was defined as when the vertical position first reached 99% of the peak vertical position of the aligned best scaled $\mathbf{x}_{nom}$. Note that the end of the trial was not defined by a stand still.

2.4 Experimental set-up

The experiment consisted of two parts: motion capture and capacity measurements. These parts were measured in parallel with two participants at the same time. There was a large amount of recovery time between the tests so we assume we can neglect effects of fatigue. For this study, we only look at the data from the motion capture experiment.

2.4.1 Sit-to-stand motion capture

We used a VICON (VICON, 2019) motion capture system with ten cameras recording at 100 Hz to capture the motion trials. Participants were equipped with 84 reflective markers of 14 mm-diameter spherical markers to the thorax, arms, pelvis, legs and feet with double-sided adhesive tape. A full description of the marker set and the fourteen segment body-model is in Appendix A. The seat height was set such that the thigh was parallel to the ground with an approximate deviation of 5º. For the thigh push-off trials additional small portable force plates were attached to the palms of the hand to measure the contact force during thigh push-off. For this study, we did not use the force data of the small portable force plates.

The participant had to perform two sets of three successful sit-to-stand trials:

- Thigh push-off (TH): the participant had to push off pressing their hands on their thighs.
- No thigh push-off (N): the participant was instructed to repeat sit-to-stand without using arms to push off.

In both sets there was no further restriction in sit-to-stand style: no posture instructions, arm placement instructions, no restriction in feet position,the speed and time between trials was self-selected and the use of arm swing was to the preference of the participant.

Post-processing and analysis were performed in MATLAB2020b with use of the VU3D-model toolbox (Sjoerd Bruijn, 2018). Outliers, marker data with an absolute value larger than 50m, were removed. We used piecewise cubic spline interpolation to fill gaps in marker data up to 10 frames. Position data was filtered using a 6th-order Butterworth filter with a cut-off frequency of 2Hz.

2.4.2 Participants

This study comprised 27 young (Y) (aged 20-35, 13 men and 14 women) and 23 healthy older (E) adults (aged 65-95, 11 men and 12 women) recruited between July and November 2019 in London, UK. Participants were excluded if the participant had joint surgery or suffered from any mobility-limiting pathology, had a pacemaker, was not able to walk without aid, was too inadequate in English to comprehend instructions or question forms, had an allergy to adhesives, was pregnant or was identified as 'moderately' or 'severely' frail at the Edmonton Frailty Scale[16]. The Imperial College institutional ethics committee approved the study. All participants gave their informed consent. Eleven participants were excluded from the data as the sit-to-stand data was incomplete and no stability basin could be computed. The final set of participants for this study comprises 39 participants, divided by age and sex into four groups, as presented in Table 1.

	n	Age [y] M (SD)	BMI [kg/m^2] M (SD)
Young Male (YM)	9	26.44 (4.09)	24.14 (2.73)
Young Female (YF)	13	27.23 (5.01)	22.82 (2.98)
Elderly Male (EM)	7	76.43 (7.98)	24.97 (3.45)
Elderly Female (EF)	10	75.90 (5.39)	24.83 (3.81)

Table 1 Participant overview

2.5 Analysis

We performed between-group and between-strategy analysis on the computed basins to study the effects of thigh push-off on stability for young and elderly subjects. We studied the accuracy of the computed stability basins by calculation of the relative volume.

2.5.1 Accuracy stability basin

The resulting stability basins describe the possible trajectories that reach successful standing without a change of strategy. However, the pendulum model and fitted controller are not a perfect representation of reality. Underestimation of the true stable region is a common phenomenon using stability basins. Holmes[17] observed false failure prediction in 76.96% of the measured trials using the LQR controller. We speak of false failure prediction when observed successful trajectories lay outside the computed stability basin. Because the stability basins are not perfect, we have to quantify the accuracy of our computed stability basins to perform between-group and between-strategy analysis.

To assess accuracy, the resulting stability basin (SB) can be described quantitively as a percentage of the maximum possible bounded domain (IB). The bounded domain, or naive stability basin[6], is the encapsulation of all observed trajectories at each time step with the same technique we applied to obtain the target set (*section 2.1.3*).

$$relative\ volume = \frac{1}{200} \bullet \sum_{i} \frac{SB(t_i)}{IB(t_i)} * 100\%$$

Where $\boldsymbol{i} \in [1,200]$; an index for each zonotope describing the stability basin. $\boldsymbol{t_i} = [0,1]$ [1x200].

A relative volume of 0% indicates that the bounded domain, and therefore all observed trajectories, lie outside the stability basin for the entire sit-to-stand movement. 100% indicates the bounded domain, and therefore all observed trajectories, remains within the computed stability basin for the entire trial.[5] A relative volume of 40% indicates that 40% of the bounded domain, and therefore 40% of all observed trajectories, lies inside the computed stability basin. The false failure prediction is 60% as 60% of the observed successful trajectories lay outside the stability basin.

2.5.2 Statistical Analysis

The computed stability basins have a total volume, or size. This can be interpreted as an overall metric of stability of the observed sit-to-stand movements. Conform the study of Shia et al.[5] we compared the total volume of the stability basins of the no-arm strategy with the thigh push-off strategy with a paired t-test. We compared no-arm (N) basins with thigh push-off (TH) basins for all participants, within age-gender group (young male N compared to young male TH etc) and for young and elderly participants separately (young N compared to young TH etc). To study age- and gender group differences we compared the basin sizes of the no-arm strategy basins of the young participants (Y-N) with the sizes of the no-arm strategy basins of the elderly participants (E-N), likewise for the thigh push-off basins (Y-TH compared to E-TH).

Compared to other stability analyses, the stability basin enables to assess the stability *throughout the movement* by assessing the stability basin's shape. To identify momentary differences in stability, we used statistical parametric mapping (SPMD). SPMD allows to study statistical differences in continuous datasets. The mapping method makes interferences of statistical processes that are continuous functions on topological features using Random Field Theory (Pataky, 2021). We assessed the size of the stability basin as a continuous function through time interval [0,1]. Specifically, the volume of the stability basin through the sit-to-stand time ($\boldsymbol{V_{SB}(t)}$ [m^4]), or the area in either the forward or upward direction ($\boldsymbol{Ax(t)}$ [m^2] or $\boldsymbol{Ay(t)}$ [m^2]) acted as the continuous one-dimensional data. We used open-access MATLAB package spm1d (Pataky, 2021) which applies SPMD to one-dimensional data. We performed a SPMD analysis of variance (ANOVA) to compare the stability basin shapes between arm-strategies (independent of age or gender) and between age groups for each

arm-strategy (young compared to elderly). The SPM(t) value indicates the momentary chance that the continuous data is different for the observed groups. We compared the continuous data of sit-to-stand with- and without thigh push-off (N/TH) and between age groups for both arm-strategies (Y/E N and Y/E TH).

To study the correlation of the stability basin size and other known individual-specific parameters we performed linear regression analyses. We analysed the correlation of basin size to age, the target set area [m^4], mean sit-to-stand time [s] and average centre-of-mass acceleration range [m/s^2].

For all statistical analyses the confidence interval was set to 95%.

3 Results

In this section we present examples of computed stability basins, show the range of accuracy of the computed stability basins, and compare the basins between arm-strategies and between age-groups.

We computed two stability basins for 39 participants, one for sit-to-stand with thigh push-off (TH) and one for sit-to-stand without thigh push-off (N). In figure 5 we present two examples of computed stability basins. A stability basin is visualised as two volumes: one for the possible trajectories depended on time in mediolateral direction ($\mathbf{r_x(t)}$, $\mathbf{v_x(t)}$), and one for the possible trajectories depended on time in upward direction ($\mathbf{r_y(t)}$, $\mathbf{v_y(t)}$). Where the basin is large there are more possible trajectories that reach standing without a change in strategy; for this observed sit-to-stand strategy the strategy is (momentarily) more stable.

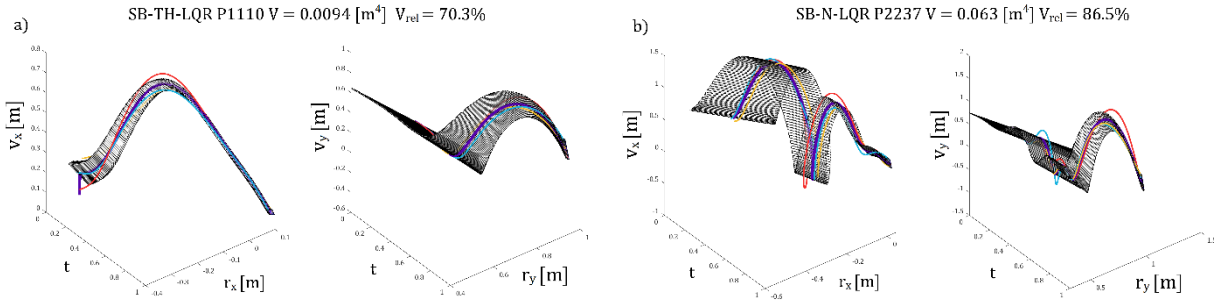

Figure 4 Two examples of computed stability basins. a) stability basin of a young female participant for sit-to-stand without thigh push-off (N) b) stability basin of an elderly male participant without thigh push-off (N). Each basins is presented separately for the anterior-posterior (left) and upward (right) component of sit-to-stand.The red, yellow and blue line represent the observed trajectories, the purple line the average nominal trajectoy.

3.1 Accuracy or relative volume

Note that, in figure 5, part of the observed trajectories lie outside the stability basin indicating that, in theory, the observed trajectories could not reach standing without a change of sit-to-stand strategy (change of feedforward control). However, all the observed trajectories reached standing successfully. Thus, we observe false failure prediction. The stability basin underestimates the true stable region. The accuracy of the computed basins, described by the relative volume of the enclosed trajectories (section 2.5.2), has a median of 86.25% and a standard deviation of 19.00% for all computed basins. In figure 6 we present a boxplot of the computed accuracies per arm-strategy, separately for young and elderly participants. The difference in accuracy between thigh push-off stability basins and no-arm stability basins is not significant: The difference in accuracy between the stability basins of the elderly and the stability basins of the young participants is not significant: $V_{rel\_N\_Y}$ = 79.0 ± 24.2 [%], $V_{rel\_N\_E}$ = 85.0 ± 14.0 [%], $p_{rel\_N\_E/Y}$ = 0.375, $V_{rel\_TH\_Y}$ = 78.8 ± 19.1 [%], $V_{rel\_TH\_E}$ = 81.3 ± 17.0 [%], $p_{rel\_TH\_E/Y}$ = 0.671. Neither is the difference in accuracy between thigh push-off and no-arm sit-to-stand: $p_{rel\_Y\_TH/N}$ = 0.975, $p_{rel\_E\_TH/N}$ = 0.504.

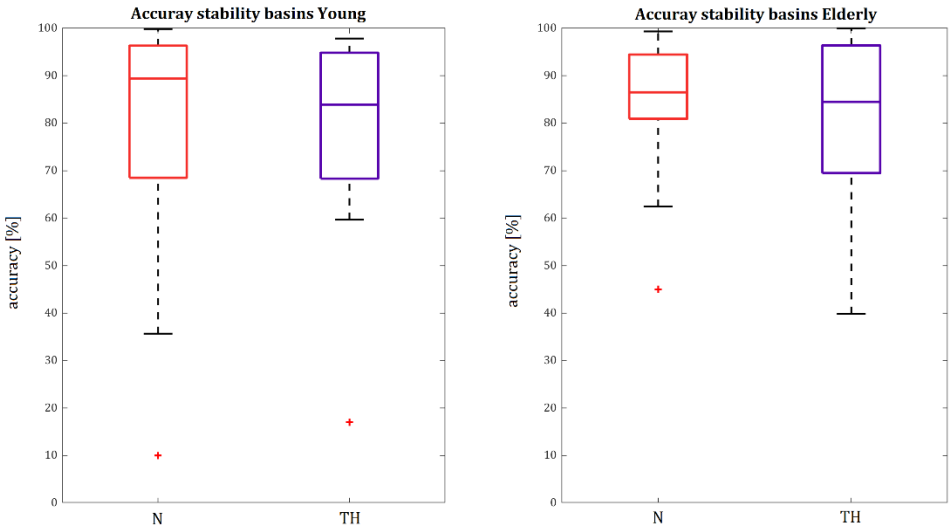

Figure 5 Boxplots of the accuracy (relative volume) of the computed stability basins per arm-strategy and age-group

3.2 Arm-strategy comparison

In table 2 we present the mean values of the size of the stability basins per age- and gender-groups per arm-strategy.

	#	N_mean	N_sd	TH_mean	TH_sd	TH > N ?	$p_{TH>N}$
All	39	0.0083	0.0123	0.0404	0.0870	28/39	0.025
Young	22	0.0062	0.0103	0.0159	0.0437	15/22	0.319
Young Male	9	0.0037	0.0036	0.0264	0.0687	5/9	0.337
Young Female	13	0.0080	0.0130	0.0086	0.0074	10/13	0.879
Elderly	17	0.0109	0.0144	0.0722	0.1165	13/17	0.039
Elderly Male	7	0.0157	0.0216	0.0482	0.0559	5/7	0.178
Elderly Female	10	0.0075	0.0051	0.0890	0.1458	8/10	0.094

Table 2 Stability basin sizes per participant group [m4] for thigh push-off (TH) and no-arm push-off (N). The pre-final column shows the number of individuals for which the stability basin of the thigh push-off was larger than for the no-arm strategy.

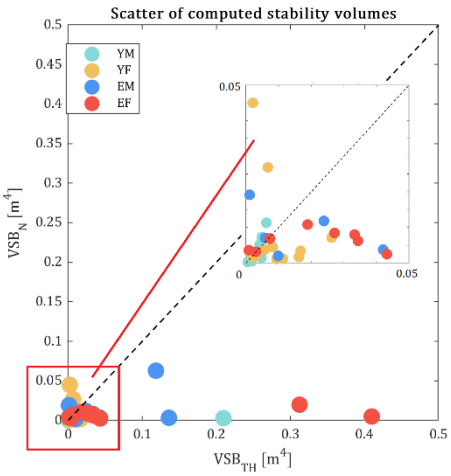

Figure 7 Scatter of the computed stability basin sizes for both arm strategies per subject. Colors indicate agegender group.

If we consider all participants, the size of the computed stability basin for thigh push-off (TH) was significantly larger than for no arm push-off (N): N = 0.0083 ± 0.0123 [m^4], TH = 0.0404 ± 0.0870 [m^4], p = 0.025. The size difference is not significant within age-gender groups alone. The size difference is larger for elderly than for young participants. Note, if we look at the means in table 2, that this difference is small for the young female participant groups. This is due to two young females with a large no-arm-strategy stability-basin (V_N_P1108 = 0.027 m^4, V_N_P1130 = 0.045 m^4). With the no-arm-strategy, both of these participants showed non-fluent sit-to-stand with hitches; a point in sit-to-stand when the velocity of the centre of mass became negative in both the vertical direction. This hesitation was consistent over the three observed trials.

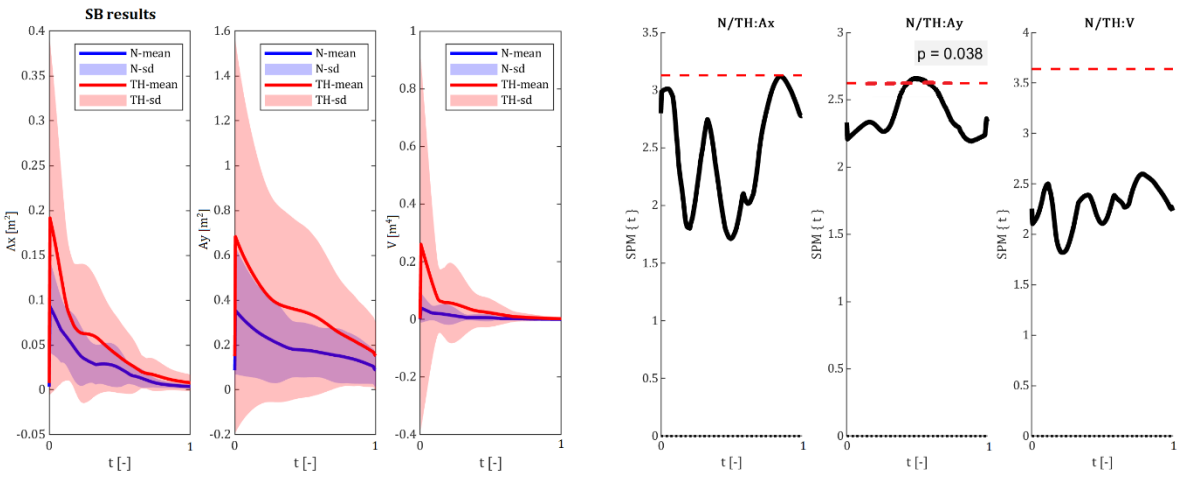

Figure 8 SPMD analysis comparison shape of stability basins (SB) for sit-to-stand with (TH) and without (N) thigh push-off independent of age- or gender groups.

SPMD analysis shows the difference between strategies in the size of the stability basin is largest, and significant, in the vertical direction in the middle of sit-to-stand ($p = 0.038$). See figure 8.

3.3 Participant-group comparison

Overall, the stability basins of the elderly were larger compared to those of the young participants, for both arm strategies. $V_{N\_Y} = 0.0062 \pm 0.0103$ [m^4], $V_{N\_E} = 0.0109 \pm 0.0144$ [m^4], $p_{N\_E/Y} = 0.249$, $V_{TH\_Y} = 0.0159 \pm 0.0437$ [m^4], $V_{TH\_E} = 0.0722 \pm 0.1165$ [m^4], $p_{TH\_E/Y} = 0.044$. For stability basins of sit-to-stand with thigh push-off the elderly have a significantly larger stability basin than the young participants. For sit-to-stand without arm push-off, this difference is not significant. Note: if we excluded outliers P1108 and P1130, the two young females with hesitant sit-to-stand without thigh push-off, the stability basins of the elderly are significantly larger than the stability basins of the young participants: $V_{N\_Y\_exP8\&30} = 0.0033 \pm 0.0027$ [m^4], $V_{N\_E\_exP8\&30} = 0.0109 \pm 0.0144$ [m^4], $p_{N\_E/Y\_exP8\&30} = 0.026$.

As presented in figure 9, SPMD analysis shows the significant differences in shape between elderly and young for each arm-strategy. The no-arm strategy shows points in sit-to-stand where the elderly's basins are significantly larger *in the horizontal plane* compared to those of the young participants: at the start of sit-to-stand and just after the peak vertical velocity. The stability basins of the thigh push-off strategy show a significant difference where the elderly have a larger basins compared to the young participants at the start of sit-to-stand. The dashed vertical lines indicate the mean sit-to-stand phase transitions[18] between primary horizontal movement to primary vertical movement.

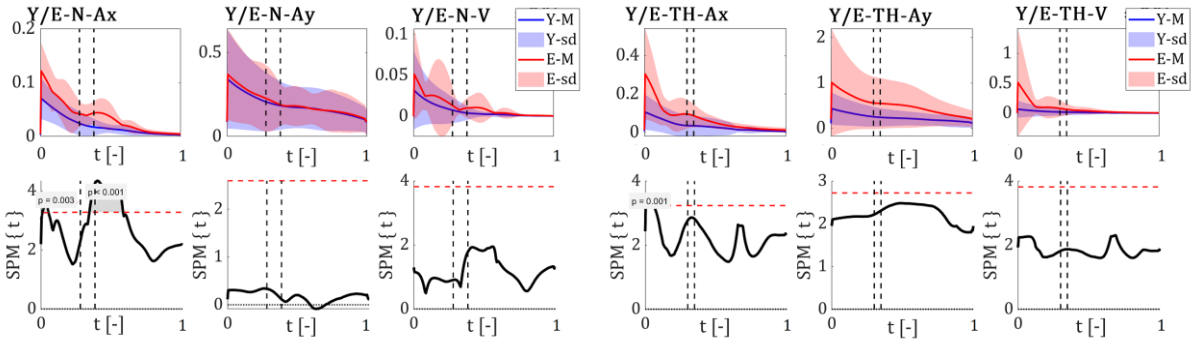

Figure 9 SPMD age-group-analysis. The vertical black striped lines indicate the mean phase transitions of the sit-to-stand observations. Sit-to-stand can be described in three phases: the accelerating phase (I), the transition phase (II) and the deceleration phase (III). Where the SPM(t) reaches the threshold the difference in the size of stability basins are momentarily significant.

3.4 Regression analysis

In appendix D we present visual presentations of the regression analyses.

Regression analysis showed that slower (larger average end time sit-to-stand) and inconsistent (large target set area) sit-to-stand is correlated to a larger stability basin independent of arm-strategy ($p_{Ntend} < 0.001$, $p_{THtend} < 0.001$, $p_{NATs} = 0.010$, $p_{THATs} = 0.015$).

Regression analysis showed that smoother (smaller mean absolute acceleration range) sit-to-stand is stronger correlated to a smaller stability basin for sit-to-stand without thigh push-off than for sit-to-stand with thigh push-off ($p_{Naccrange} < 0.001$, $p_{THaccrange}=0.070$).

We found a weak positive linear correlation to the stability basin size and age ($p_{Nage} = 0.095$, $p_{THage} = 0.167$).

4 Discussion

We hypothesised that sit-to-stand with thigh push-off is more stable than sit-to-stand without thigh push-off, in young and elderly participants. We found that the stability basins for sit-to-stand with thigh push-off are larger than for sit-to-stand without push-off, for most (29/39) participants. Over all participants, the stability basin of the thigh push-off was significantly larger than the basins of the no-arm sit-to-stand strategy. The basin size difference between arm-strategies were larger for the elderly participants than for the young participants. The differences in the shape of the stability basins between young and elderly were different for the two arm-strategies: without thigh push-off basins were larger for elderly at the middle (40-60% of movement) and start of sit-to-stand (0-10% of movement), with thigh push-off basins only at the start of sit-to-stand. Accuracy of the stability basin, estimated by relative volume, was high (compared to previous studies) and even over the four age-gender groups.

Accuracy The accuracy of the computed stability basins is lower than 100%, thus we observe underestimation of the true stable region. This means the computed stability basins cannot predict the actual limits of the observed strategies. However, we showed that the accuracy of the computed stability basins is comparable over all participant- and strategy groups such that between-age and between-strategy stability basin comparison is valid. Furthermore, the underestimation is small compared to the study of Shia[5] where they successfully distinguished differences in stability between two restricted sit-to-stand strategies.

The accuracy, or relative volume, of a stability basin is largely dependent on controller fit. We optimised the feedback and feedforward control parameters such that they best fitted the observed sit-to-stand centre-of-mass trajectories. With the linear quadratic controller we use, accuracies of near 100% can only be obtained if all measured trajectories fit a linear model. To achieve better accuracy, Holmes[6] introduced a more sophisticated controller model where the controller input is defined as a range of inputs fitting the observed data thereby modelling a range of inputs which predict successful standing. In Holmes' perturbation study, the input bound controller reduced false failure prediction from 76.96% to 15.02% compared to the linear quadratic controller (LQ)R controller.[17] In our study, we only had three observations to form a stability basin on. The fabrication of 'extra points' in the target set nearby the observed end points mathematically enabled us to compute the stability basins. Adversely, the target set area became very small and the stability basins become more of a slab than a volume. This raises concerns about overparametrisation. We checked available control models and found that only the LQR controller did not show signs of overparameterising for an input of three observations. In appendix E we present the results of this check.

Our high accuracy score, compared to the previous studies, partly can be explained by the small number of trials we based our model on. A linear model based on three inputs can fit more accurately to those three inputs compared to a model with five (Shia[5]) up to twelve (Holmes[6]) trials used as input for previous studies. However, we had a higher chance of more variable observations as we studied novel unrestricted sit-to-stand data, where the other studies used restricted (instructions on execution) sit-to-stand. More variable but successful observations result in a larger basin but also a worse controller fit and thus lower accuracy

Between-strategy. The stability basins of thigh push-off strategy sit-to-stand were overall larger than for the no-arm strategy. A larger basin indicates there are more possible trajectories that reach standing following the observed sit-to-stand strategy. In other words, in the observed thigh push-off sit-to-stand strategies was more room for variation and a larger resistance to small perturbations; the strategy was more stable. That said, it is not the case for all participants.

In this study we analysed unrestricted sit-to-stand. Participants were free to execute sit-to-stand to their preference. The chosen observed style, where use of trunk flexion is a characteristic for example,

largely influences the stability. Shia[5] showed for all participants that the stability basins indicated one instructed strategy (quasi-static) to be more stable than another (momentum transfer). Because, in our study, there were no restrictions in sit-to-stand style except for arm-use the observed strategies show between- participant and between-arm strategy variability. This could have lead to a participant performing a careful and stable version of sit-to-stand without thigh push-off and a hastily executed thigh push-off sit-to-stand, if that was to their preference. The observed natural strategies indicate that for some individuals thigh push-off sit-to-stand is less stable. This could be due to a number of irregularities in the observatios e.g. alternate foot placement, between-strategy variation in intention of the participants (unconciously chosen different movement objectives), undetected asymmetry or the participants being distracted. However, we wanted to study natural sit-to-stand. And these irregularities can be typical of the participant's natural sit-to-stand style for the instructed arm-strategies. Therefore we did not exclude these results.

Because the difference in stability basin size is significant between the two strategies and the participants with a more stable sit-to-stand without thigh push-off are distributed evenly over the participant groups, we conclude that sit-to-stand with thigh push-off is, in general, likely to be more stable than sit-to-stand without thigh push-of.

Between-group Between-group analysis shows that the stability basins of the elderly are larger compared to those of the young participants. This indicates that elderly use more stable sit-to-stand strategies. These results contradict our hypothesis that elderly have a smaller basin because we assumed elderly to be more unstable. This reveals the explicit statement that stability basins quantify the *stability of the observed movements rather than the stability of the observed subject*. What we observed is that elderly's observed strategy has more room for variation in it's simulated trajectories to still reach standing within the observed strategy. And more room for variation is a higher resistance to small perturbations. Intuitively, this is understandable. Elderly have a decreased neuromuscular capacity[19] and are therefore less capable of a successful (quick) change of strategy which could result in falling. To reduce this risk elderly use more careful strategies; with more room for variation before a necessary (possible risky) change of strategy.

The shape analysis further strengthens this conclusion. We observed a larger basin for the elderly at specific points in sit-to-stand which indicate that, compared to the young participants, the strategy used by elderly has more room for error at those points. In other words: they were more careful at these specific points. If we assume humans to be optimisers caution is only taken when necessary, to reduce risks or even avoid specific failures. For the thigh push-off there is one significant point of difference, where the elderly basins are significantly larger than the young participants' basins, at the start of sit-to-stand; compliant with a failure mode of an early sit-down. For sit-to-stand without thigh push-off there is a second and larger difference in basin size halfway sit-to-stand; compliant with a failure mode of a sit-down or step in the transition phase and the start of the deceleration phase[18]. The consequences of a step or sit-down in the later stages of sit-to-stand have more risks than an early sit-down. This implicates that thigh push-off is not only in general a more stable strategy, as quantified by the overall larger basin size, but also that it is a strategy with lower risks if the subject needs to change the strategy.

Regression analysis We found a strong positive correlation to the stability basin size and the average mean end time of sit-to-stand and the target set area. One could argue that these values alone can act as an overall metric of stability. This would eliminate the need of the model fitting and simulation and would reduce the method to just the data pre-procesment, specifically trial segmentation using the average nominal trajectory. However, the average end time and end point consistency do not give any information about the stability throughout the movement. This remains an essential advantage of the stability basin method. The strong positive correlations do confirm that the computed stability basin sizes act a stability metric as they correlate to logical other stability indicators, speed and consistency, independent of arm-strategy.

The correlation to the range of centre of mass acceleration during the movement (mean value over three observations) is significanlty stronger for the no-arm strategy than the thigh push-off strategy. Interestingly, for the no-arm strategy the observed acceleration range was smaller and with less variation compared to the observed acceleration range of the thigh push-off strategy (see Appendix D, figure 17). The larger variation and range in centre-of-mass acceleration for thigh push-off did not result in a larger variation and size of the stability basin for the thigh push-off. This indicates that the stability of sit-to-stand using thigh push-off is less dependent on the acceleration of the centre of mas. This could mean that thigh push-off sit-to-stand can be executed with a higher speed and less control, or slower speed and more control, with less influence on the stability than it would have if no arms were used. This stability robustness, if we may call it such, could explain why elderly frequently prefer thigh push-off sit-to-stand over using no arms in sit-to-stand.[3]

Future recommendations Some critical notes on the use of stability basins. If the predictive power of the basins is insufficient the potential of the method is limited. For future effective use of stability basins we recommend an accuracy study of stability basins and the different models of controllers dependent on the number of trials and variability of the input. This could be performed by using available sit-to-stand data sets (from the Holmes[17] perturbation study for example) and leaving multiple trajectories out or as a simulative study, where the 'observed' trajectories are simulated using a musculoskeletal model to obtain realistic input data.

If the predicitve power can be improved there are multiple applications and improvements to be further made using stability basins. We only studied the stability of sit-to-stand with and without thigh push-off. With the stability basin method one could easily study the stability of other common sit-to-stand strategies, such as using arm rests. With the simple inverted pendulum model and the neglection of angular momentum there would be no need to adjust the equations of motion, even if arm rests are used. Another movement which could be studied with stability basins is sit-to-walk. For other stability quantification methods, the end point of the aperiodic sit-to-walk movement can be difficult to define as the 'end point' is walking, a non-stationary position. With the stability basin method this would be defined by the target set which simply could be all the observed trajectory points at the moment of the second heel strike for example.

Furthermore, to improve understanding in the stability of certain movement strategies, the stability basin is fit to be extended to include medio-lateral stability assessment as well. One would need to add another dimension, one state variable for centre of mass lateral position and one state variable for centre of mass lateral velocity, which would result in a six-dimensional stability basin. The stablity basin would be visualised in three volumes instead of two. The total size of the stability basin, acting as overall stability metric of the entire movement, would be more correlated to the 'actual' stability, in terms of risk of falling, of the movement.

Both Shia et al.[5] and Holmes et al.[6] proposed to use the stability basin method in longitudinal studies to track the influence of age or (the rehabilitation) of an injury on instability. The stability basin should be able to reveal unstable portions of motion. Coupling with other clinial techniques, such as electromyography, stability basins could help to indentify which (weakened) muscles are associated with (momentary) instability. This could improve preventitive and rehabilitive care.[5,6] However, our results based on unrestricted sit-to-stand movements showed that the stability basins quantify the stability of the observed chosen movement *strategy*. An example: Longitudinal studies using stability basins could show decreased momentary stability according to the stability basins. This would indicate that the observed strategy has an increased chance of a *necessary change of strategy* to avoid failure. However, if studying unrestricted strategies, this would not necessarily mean an increased likelyhood of falling and therefore indicating decreased stability. It could also show that the subject has a decreased fear of falling and therefore uses a more 'risky' strategy now, indicating increased stability. Therefore, we recommend to only use stability basins in longitudinal studies with restricted movement strategies. For unrestricted statregies, one should couple the results with other clinical (stability) assesments. Then, the stability basins could aid to understand strategy preferences.

5 Conclusion

We conclude that, in general, sit-to-stand with thigh push-off is likely to be a more stable strategy than sit-to-stand with no arms: The computed stability basins show that the thigh puh-off strategy is more robust to small perturbations to reach standing without a change in strategy for most of the observed natural strategies. Compared to those of young adults, the observed older adults strategies have less risk for a possible early sit-down and a step mid sit-to-stand in sit-to-stand without thigh push-off and only for early sit-down for the thigh push-off strategy. The differences in stability basin size between the elderly and young participants confirm that stability basins quantify the stability of the observed movement strategy rather than the stability of the subject.

References

1. Florence, Curtis S. Gwen Bergen AA. The Medical Costs of Fatal Falls and Fall Injuries among Older Adults. *Am Geriartics Soc*. 2018;66(4):693-698. doi:doi:10.1111/jgs.15304

2. Frykberg GE, Häger CK. Movement analysis of sit-to-stand–research informing clinical practice. *Phys Ther Rev*. 2015;20(3):156-167. doi:10.1179/1743288X15Y.0000000005

3. van der Kruk E, Silverman AK, Reilly P, Bull AMJ. Compensation due to age-related decline in sit-to-stand and sit-to-walk. *J Biomech*. 2021;122:110411. doi:10.1016/j.jbiomech.2021.110411

4. Bruijn SM, Meijer OG, Beek PJ, Van Dieen JH. Assessing the stability of human locomotion: A review of current measures. *J R Soc Interface*. 2013;10(83). doi:10.1098/rsif.2012.0999

5. Shia V, Moore TY, Holmes P, Bajcsy R, Vasudevan R. Stability basin estimates fall risk from observed kinematics, demonstrated on the Sit-to-Stand task. *J Biomech*. 2018;72:37-45. doi:10.1016/j.jbiomech.2018.02.022

6. Holmes PD, Danforth SM, Fu XY, Moore TY, Vasudevan R. Characterizing the limits of human stability during motion: Perturbative experiment validates a model-based approach for the Sit-to-Stand task. *R Soc Open Sci*. 2020;7(1). doi:10.1098/rsos.191410

7. Kuo AD. An Optimal Control Model for Analyzing Human Postural Balance. *IEEE Trans Biomed Eng*. 1995;42(1):87-101. doi:10.1109/10.362914

8. Todorov E, Jordan MI. Optimal feedback control as a theory of motor coordination. *Nat Neurosci*. 2002;5(11):1226-1235. doi:10.1038/nn963

9. Pisotta I, Molinari M. Cerebellar contribution to feedforward control of locomotion. *Front Hum Neurosci*. 2014;8(JUNE):1-5. doi:10.3389/fnhum.2014.00475

10. Lancaster P, Rodman L. The Algebraic Riccati Equation. In: *The Algebraic Ricatti Equation*. Vol 14. New York, NY: Oxford Univeristy Press.; 1995.

11. Althoff M, Stursberg O, Buss M. Reachability analysis of nonlinear systems with uncertain parameters using conservative linearization. *Proc IEEE Conf Decis Control*. 2008:4042-4048. doi:10.1109/CDC.2008.4738704

12. Merrill Z, Perera S, Chambers A, Cham R. Age and body mass index associations with body segment parameters. *J Biomech*. 2019;88:38-47. doi:10.1016/j.jbiomech.2019.03.016

13. Catena RD, Chen SH, Chou LS. Does the anthropometric model influence whole-body center of mass calculations in gait? *J Biomech*. 2017;59:23-28. doi:10.1016/j.jbiomech.2017.05.007

14. Leva P De. Adjustments to Zatsiorsky-Seluyanov's segment inertia parameters. *J Biomech*. 1996;29(9):1223-1230.

15. Pavol MJ, Owings TM, Grabiner MD. Body segment inertial parameter estimation for the general population of older adults. *J Biomech*. 2002;35(5):707-712. doi:10.1016/S0021-9290(01)00250-0

16. Jankowska-Polańska B, Uchmanowicz B, Kujawska-Danecka H, et al. Assessment of frailty syndrome using Edmonton frailty scale in Polish elderly sample. *Aging Male*. 2019;22(3):177-186. doi:10.1080/13685538.2018.1450376

17. Holmes PD, Danforth SM, Fu XY, Moore TY, Vasudevan R. Characterizing the limits of human stability during motion: Perturbative experiment validates a model-based approach for the Sit-to-Stand task. *arXiv*. 2019.

18. Roebroeck ME, Doorenbosch CAM, Harlaar J, Jacobs R, Lankhorst GJ. Biomechanics and muscular activity during sit-to-stand transfer. *Clin Biomech*. 1994;9(4):235-244. doi:10.1016/0268-0033(94)90004-3

19. van der Kruk E, Silverman AK, Koizia L, Reilly P, Fertleman M, Bull AMJ. Age-related compensation: Neuromusculoskeletal capacity, reserve & movement objectives. *J Biomech*. 2021;122(March):1-13. doi:10.1016/j.jbiomech.2021.110385

20. Meunier P, Yin S. Performance of a 2D image-based anthropometric measurement and clothing sizing system. *Appl Ergon*. 2000;31(5):445-451. doi:10.1016/S0003-6870(00)00023-5

21. Powell-Tuck J, Hennessy EM. A comparison of mid upper arm circumference, body mass index and weight loss as indices of undernutrition in acutely hospitalized patients. *Clin Nutr*. 2003;22(3):307-312. doi:10.1016/S0261-5614(03)00009-8

22. Zatsiorksy V, Seluyanov V, L C. In vivo body degment inertial parameters determination using a gamma-scanner method. 1990:186-202.

23. Pavol MJ, Owings TM, Grabiner MD. Body segment inertial parameter estimation for the general population of older adults. *J Biomech*. 2002;35:707-712.

24. Yeadon MR. The simulation of aerial movement-II. A mathematical inertia model of the human body. *J Biomech*. 1990;23(1):67-74. doi:10.1016/0021-9290(90)90370-I

25. Vaughan C., Davis B., O'Connor J. *Dynamics of Human Gait*. 2nd ed. (Vaughan C, ed.). Cape Town, South Africa: Kiboho Publishers; 1992.

26. Plagenhoef S, Gaynor Evans F, Abdelnour T. Anatomical Data for Analyzing Human Motion. *Res Q Exerc Sport*. 1983;54(2):169-178. doi:10.1080/02701367.1983.10605290

27. Bell AL, Pedersen DR, Brand RA. A comparison of the accuracy of several hip center location prediction methods. *J Biomech*. 1990;23(6):617-621. doi:10.1016/0021-9290(90)90054-7

28. Leardini A, Cappozzo A, Catani F, et al. Validation of a functional method for the estimation of hip joint centre location. *J Biomech*. 1999;32(1):99-103. doi:10.1016/S0021-9290(98)00148-1

29. Reynolds HM. Spatial Geometry of the Human Pelvis. *Fed Aviat Adm Washingt DC*. 1982;(March).

Websites and toolboxes

1. *Belstaff Men's sizing Chart*. (2020, Mei). Opgehaald van Belstaff.eu: https://www.belstaff.eu/en/customer-service/mens-sizing-chart.html

2. *BMI and obesity: Where are you on the UK fat scale?* (2018, April 24). Opgehaald van BBC Health: https://www.bbc.com/news/health-43697948

3. Pataky, T. (2021, Maart). *spm1d*. Opgehaald van https://spm1d.org: https://spm1d.org/index.html

4. Sjoerd Bruijn, I. K. (2018). VU-3D-model.

5. VICON. (2019). Vicon Motion Systems Ltd UK registered no. 1801446.

Appendices

A – Full marker set description

Segment	Markers	Anatomical Location
Foot – left and right	FM2	Head of the second metatarsal
	FCC	Calcaneus
	FMT	Tuberosity of the fifth metatarsal
	TF	Additional marker placed on foot
Calf - left and right	TAM	Apex of the medial malleolus
	FAM	Apex of the lateral malleolus
	C1-4	Cluster of four markers placed on frontal flat part of the shank
Thigh – left and right	FLE	Lateral femoral epicondyle
	FME	Medial femoral epicondyle
	T1-4	Cluster of four markers placed on lateral side of thigh
Pelvis	RASIS	Right anterior superior iliac spine
	LASIS	Left anterior superior iliac spine
	RPSIS	Right posterior superior iliac spine
	LPSIS	Left posterior superior iliac spine
	P1-3	Cluster of three markers placed on pelvis
Thorax	C7	7th cervical vertebra
	T8	8th thoracic vertebra
	IJ	Sternum jugular notch
	MA	Sternum manubrium
	PX	Sternum xiphoid process
	LS1	Left acromion
	RS1	Right acromion
Upper arm – left and right	LE	Lateral epicondyle
	ME	Medial epicondyle
	HU1-4	Cluster of four markers placed on lateral side upper arm
Lower arm – left and right	RS	Radial styloid
	US	Ulnar styloid
	U1-4	Cluster of four markers placed on lateral side thigh

Table 2 Full marker-set description

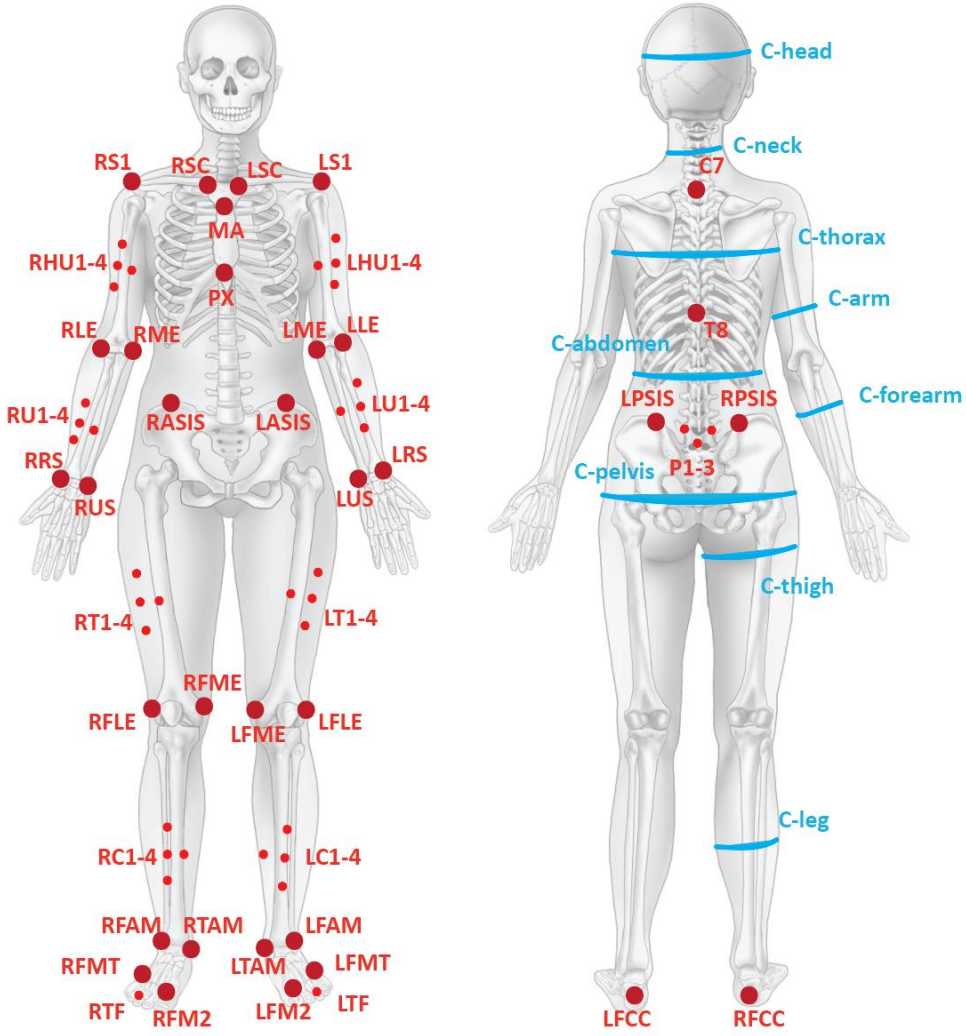

Figure 6 Overview full marker-set and circumference locations

B - Anthropomorphic model

This section elaborates on anthropomorphic model choices.

Circumference Approximation

Circumferential data largely accounts for the between-subject variation. Approximation of circumferences from photos of participants developed for the clothing industry [20] had limited application without the availability of photos of the transverse plane. To vary the approximated circumferences on the individual's Body Mass Index (BMI) we can account for up to 50% of the between-subject variability of the BSPs[12]. For each circumference approximation we assume a linear relation between BMI and circumferences. A first degree polynomial was used to fit known correlations between BMI and circumferences. The circumferences of the pelvis, abdomen and thorax were derived from a standard UK size chart (Belstaff Men's sizing Chart, 2020) where we assumed the underweight boundary of a BMI of 18 to correspond with a size XS and the overweight boundary BMI of 30 to correspond to XL for female. The XL waist circumference corresponded to the waist circumference of 80 cm which is another indicator for overweight. (BMI and obesity: Where are you on the UK fat scale?, 2018) For the male group, a similar approach resulted in size XS and XL corresponding to a BMI of 20 an 32 kg/m^2 respectively. These known correlations are presented in table 4.

		Male values		Female values	
		min	max	min	max
	BMI (kg/m^2)	18	28	18	28
Calf 7	circumference (cm)	31	42	29	40
	BMI (kg/m^2)	20.8	27	19.9	25.3
Thigh 8	circumference (cm)	53.2	65.6	48.1	57.5
	BMI (kg/m^2)	20	32	18	30
Pelvis	circumference (cm)	91	107	90	106
	BMI (kg/m^2)	20	32	18	30
Abdomen	circumference (cm)	78.5	94.5	64	80
	BMI (kg/m^2)	20	32	18	30
Thorax	circumference (cm)	90	106	82	98
	BMI (kg/m^2)	21.7	25.0	21.0	25.0
Neck 9	circumference (cm)	35.5	37.5	31.5	33.5

Table 3 BMI coefficients

The upper arm circumference is approximated with regression equations from a large study (n=408 male, n=258 female) with reasonable predictability (R^2=0.76).[21]

$$C = BMI/1.01 + 4.7 \text{ for male participants}$$

$$C = BMI/1.10 + 6.7 \text{ for female participants}$$

The feet circumferences we assumed to be BMI independent and are scaled to standard lengths dependened on gender. Both the Forearms and hands were scaled to ratio between the length of the forearm and the standard length of the forearm. The head circumference was assumed to be the same standard circumference and only gender dependent. These circumferences are presented in table 5.

$$C = C_{standard} * L/L_{standard}$$

		Standard length	Standard circumference (cm)
	male	258.1 mm	25 cm
Foot 2	female	228.3 mm	22.1 cm *assuming same ratio male
	male	268.9 mm	26 cm
Forearm 2	female	264.3 mm	25.56 cm *assuming same ratio male
	Male	*scaled to forearm ratio	21 cm
Hand 2	female	*scaled to forearm ratio	19.0 cm *assuming same ratio male
	male	-	56.9
Head 11	female	-	53.4

Table 4 Length and circumference ratio's feet, hands, forearms and head

Anthropomorphic methods

To approximate body segmental parameters (BSPs) and segment COM location a distinction in anthropomorphic models was made between the young and elderly group. The local anatomical coordinate systems of each segment were derived independent of method and participant group and are presented per segment in the subsections following the method presentation.

Zatiorsky/Leva

A method based on the studies of Zatsiorksy and de Leva[14] was used for the young subjects. Each BSP is approximated from the segmental length (L), the circumference (C) and regression parameters based on measurements with a gamma-ray scanner by Zatsiorsky et al. (1990a)[22] De Leva made adjustments so that the anthropomorphic model would depend on joint locations instead of bony landmark coordinates 'to better fit kinematic models'.[14] It is important to note what kind of participant group this method is based on. The participant group on which Zatsiorsky based his method consisted of significantly more males ($n = 100, a = 24y, 73.0kg, 1.741m$) than females ($n = 15, a = 19y, 61.9kg, 1.735m$)[22] and that the mean BMI of the male group ($24.1 kg/m^2$) is significantly higher than that of the female group ($20.6\ kg/m^2$). Equations (*eq3*) present how the mass and inertia parameters are derived for a body segment from segment length, circumference and segment specific regression parameters. K_m is the coefficient for the mass (m) derivation, K_s the coefficient for inertia parameter around the sagital axis (x-axis), and K_f and K_l for the frontal (y-axis) and longitudinal (z-axis) axis.

$$regression\ parameters\ RP = [Km, Ks, Kf, Kl]^{[14]}$$

$$m = K_m * L * C^2 * 10^{-5}$$

$$I_{xx} = I_s = K_s * m * L^2 * 10_{-2}$$

$$I_{yy} = I_f = K_f * m * L^2 * 10_{-2}$$

$$I_{zz} I_l = K_l * m * C^2 * 10_{-2}$$

Equation 3 Zatsiorksy/Leva coefficient equations

For each segment the calculation of the segment COM location approximation, segment length (L) and regression parameters are presented in the next section.

Pavol

Pavol For the elderly participant groups the Pavol[23] method was used. This method was specifically developed to estimate BSPs for the general population of older adults with a cadaver study. The study's population consisted of less male ($n = 29, a = 73.2y, 84.4kg, 1.72m$) than female ($n = 50, a = 70.3y, 71.2kg, 1.59m$) subjects.[7]

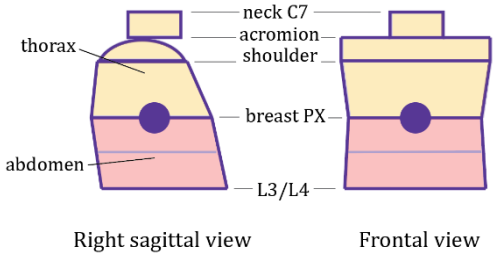

Figure 7 Adjusted Pavol model (based on five component model Yeadon) such that the thorax consists of three components and the abdomen of one component

This indicates a mean BMI value of 28.4 and 28.2 [m/kg^2] for the male and female group respectively. Pavol accounts for the large between-subject variation with individual measurements of lengths, total mass and circumferences. The trunk is modelled as five components divided by transverse sections marked by the C7, the acromion, shoulder, breast, mid breast-L3L4 and L3L4 as proposed by Yeadon[24]. We have simplified this to a four component model where the top three components together form the thorax segment and the bottom two components are modelled as one component which forms the abdomen segment. The division between the two segments is the section at the breast, indicated by the PX marker. See figure 11.

Each component is modelled as a stadium solid where the volume is approximated by a cylinder:

$$w_0 = circ_0/(\pi),\ w_1 = circ_1/(\pi)$$
$$r_0 = min(w_0, D_0) \quad t0 = max(w_0, D_0) - 2 * r_0$$
$$r_1 = min(w_1, D_1) \quad t_1 = max(w_1, D_1) - 2 * r_1$$
$$V_s = \frac{h}{3} * (2 * r_0 * t_0 + r_0 * t_1 + r_1 * t_0 + 2 * r_1 * t_1 + \pi(r_0^2 + r_0 * r_1 + r_1^2))$$

Where $circ_i$ is the circumference, w_i the width and D_i the depth at level i. Level 1 is the top level of each component, level 0 the bottom component. For example, the abdomen component $circ_1$ is the waist circumference and $circ_0$ is the hip circumference.

The depths and widths are approximated from circumferences we assumed or modelled with the assumption that the cross section is perfectly round as there was no depth data available. We calculate the thorax and abdomen COM location with the Zatsiorsky/Leva method as the assumption of a round circumference may influence the posterior location of the COM too much.

Anthropomorphic segment models

For each segment the calculation of the BSPs, the segment COM location approximation, local segment anatomical coordinate system (ACS) and segment length are presented in the next subsections. The segment specific x-, y- and z-axis axis are, for each segment, normalized to form the ACS according:

$$x_{norm} = \frac{x}{||x||} \quad y_{norm} = \frac{y}{||y||} \quad z_{norm} = \frac{z}{||z||}$$
$$gRseg = [x_{norm} \ \ y_{norm} \ \ z_{norm}] \tag{3}$$

Feet

The feet are modeled according to the adjusted Leva[14] and Pavol model[23] for young and elderly participants respectively. For the young participants the sagital axis is determined as the line of the midpoint between the head of the second metatarsal (FM2) and the tuberosity of the fifth metatarssal (FMT), and the heel (FCC). The segment length is ideally determined with a marker on the toe tip but in the absence of one we assume the total length of the foot to be 25% larger than the length between FM2 and FMT, and the heel.

Markers	Calculation ACS
1. Head of second metatarsal (FM2) 2. Tuberosity of the fifth metatarsal (FMT) 3. Calcaneous (FCC) 4. Lateral Malleolus (TAM) 5. Sphyrion (FAM) 6. Additional marker (TF)	$x_{temp} = (FM2+ FMT)/2 - CAL$ y = (FM2+FMT)/2-CAL AJC-CAL z = $x_{temp} \times y$ x = y $\times z$ $) \times ((FM2 + FMT)/2 - CAL)$
Calculated joint centres	Segment length
1. Ankle Joint Center (AJC) AJC = (TAM+FAM)/2	$L = \|\|(FM2+ FMT)/2 - FCC\|\| * 1.25$ *assumption of the extra 25%

Young participants:[23]

$$COM_{footmale} = FCC + L * 0.4415 \qquad COM_{footfemale} = FCC + L * 0.4014 \tag{4}$$

$$RP_{footmale} = [6.14\ 7.86\ 7.14\ 1.60] \qquad RP_{footfemale} = [6.35\ 8.98\ 7.79\ 2.09];$$

Elderly participants:[23,25,26]

$$COM_{foot} = AJC + 0.28 * ((FM2 + FMT)/2 - FCC) * 1.25 * cos(29.^{6}\circ) \tag{5}$$

$$COM_{foot}(3) = AJC(3) - 0.28 * L * sin(29.^{6}\circ)$$

$$m = 0.0083 * bodymass + 254.5 * L * h_{ankle} * w_{ankle} -$$

0.065[] Where $w_{ankle} = norm(SPH - LM)$ and $h_{ankle} = COM(3)$

Calfs

No adjustments were made to the models proposed by Leva[14] for young participants and Pavol[23] for elderly participants.

Markers	Calculation of Anatomical Coordinate System (ACS)
1. Lateral Malleolus (FAM) 2. Sphyrion (TAM) 3. Lateral Femur Epicondile (LFE) 4. Medial Femur Epicondile (MFE) 5-8. Four additional clustermarkers (C1-4)	$y_{temp} = MFE - LFE$ on right side $y_{temp} = LFE - MFE$ on left side z = KJC-AJC x = $y_{temp} \times z$ y = z $\times x$
Calculated joint centres	Segment length[14]
1. Ankle Joint Center (AJC) AJC = (TAM+FAM)/2 2. Knee Joint Center (KJC) KJC = (MFE+LFE)/2	$L = \|\|AJC - KJC\|\| * 393.4/440.3$ male $L = \|\|AJC - KJC\|\| * 393.8/438.6$ female

Young participants:

$$COM_{calfmale} = KJC + (AJC - KJC) * 0.4395 \qquad COM_{calffemale} = KJC + (AJC - KJC) * 0.4352 \tag{6}$$

$$RP_{calfmale} = [5.85\ 8.77\ 8.44\ 1.44] \qquad RP_{calffemale} = [6.59\ 8.80\ 8.58\ 1.42];$$

Elderly participants:

$$COM_{calfmale} = KJC + (AJC - KJC) * 0.428 \qquad COM_{calffemale} = KJC + (AJC - KJC) * 0.419 \tag{7}$$

$$m = 0.0226 * bodymass + 31.33 * L * C^2 + 0.016$$

Pelvis

Markers	Calculation ACS
1. Right Anterior-Superior Iliac Spine (RASIS) 2. Left Anterior-Superior Iliac Spine (LASIS) 3. Right Posterior-Superior Iliac Spine (RPSIS) 4. Left Posterior-Superior Iliac Spine (LPSIS) 5-7. Three additional cluster markers (P1-3) MASIS = Midpoint between RASIS and LASIS MPSIS = Midpoint between RPSIS and LPSIS	$x_{temp} = LASIS - MPSIS$ y = LASIS - RASIS $z = x_{temp} \times y$ x = y $\times z$
Calculated joint centres	Segment length[14]
1. Right Hip Joint Centre (RHJC)[27,28] See text 2. Left Hip Joint Centre (LHJC) [27,28] See text 3. Lumbar Joint Centre (LJC)[29] See text	$L = \lvert z_{navel} - z_{MHJC} \rvert * 251.7/145.7$ male $L = \lvert z_{navel} - z_{MHJC} \rvert * 256.8/181.5$ female * Navel height approximated from photos

The navel height was approximated from photos of the participants using a reference length with a known length from marker locations. Note that this was an arbitrary task whenever there was a substantial amount of body fat or loose skin. If there was no photo available the navel height was assumed to be zero. 2

$$z_{navel} = z_{MASIS} + h_{navelfromphotos} \quad \text{where} \quad navel = MASIS \tag{8}$$

Calculation joint centres:[27–29]

$$d_{pelvis} = ||(RASIS + LASIS)/2 - MPSIS|| \tag{9}$$

$$w_{pelvis} = ||RASIS - LASIS||$$

$$RHJC_{loc} = [-0.19 * w_{pelvis} \quad -0.36 * w_{pelvis} \quad -0.30 * w_{pelvis}]$$

$$LHJC_{loc} = [-0.19 * w_{pelvis} \quad 0.36 * w_{pelvis} \quad -0.30 * w_{pelvis}]$$

$$x_{RHJC} = -0.31 * d_{pelvis} \qquad x_{LHJC} = 0.31 * d_{pelvis}$$

$$Navel_{loc} = gRseg^T * (Navel - MASIS)$$

$$MPSIS_{loc} = gRseg^T * (MPSIS - MASIS)$$

$$MHJC_{loc} = RHJC_{loc} + LHJC_{loc})/2$$

$$LS51_{loc} = [-0.498888 * d_{pelvis} \quad 0 \quad 0.111790 * w_{pelvis}]_{[10]}$$

$$LS51_{loc} = [-0.543004 * d_{pelvis} \quad 0 \quad 0.102756 * w_{pelvis}]_{[10]}$$

$$RHJC = MASIS + gRseg * RHJC_{loc}$$

$$LHJC = MASIS + gRseg * LHJC_{loc}$$

$$LJC = MASIS + gRseg * L5S1_{loc}$$

Young Participants:[14,26]

$$COM_{male} = [x_{MPSIS} * 0.63 \quad 0 \quad z_{MHJC} + (z_{navel} - z_{MHJC}) * 0.3885] \tag{10}$$

$$RP_{male} = [3.60\ 10.90\ 8.92\ 0.76] \qquad RP_{female} = [3.43\ 9.37\ 8.07\ 0.74]$$

Elderly Participants:[23]

$$COM_{male} = LJC + ((RHJC + LHJC)/2 - LJC) * 0.604 \quad (11)$$

$$COM_{female} = LJC + ((RHJC + LHJC)/2 - LJC) * 0.484\ m =$$

$$K_p * bodymass + 14.61 * C + 4.2987 * (C_{waist}/C) -$$

$$11.7585$$

Where $K_p = 0.0636$ for male, $K_p = 0.0710$ for female

Thighs

No adjustments were made to the models proposed by Leva[14] and Pavol[23].

Markers	Calculation ACS
1. Lateral Femur Epicondile (LFE) 2. Medial Femur Epicondile (MFE) 3. ASIS (Not used in ACS calculation) 4-7. Four additional markers (T1-4)	$y_{temp} = MFE - LFE$ for right side $y_{temp} = LFE - MFE$ for left side z = HJC - KJC $x = y_{temp} \times z$ y = z $\times x$
Calculated joint centres	Segment length
1. Knee Joint Centre (KJC) KJC = (MFE+LFE)/2 2. Hip Joint Centre (HJC) Hip from pelvis segment, see pelvis	$L = \|\|HJC - KJC\|\| * 520.2/422.2$ for male[4] $L = \|\|HJC - KJC\|\| * 496.2/368.5$ for female

Young participants:[5]

$$COM_{thighmale} = HJC + (KJC - HJC) * 0.4095 \qquad COM_{thighfemale} = HJC + (KJC - HJC) * 0.3612 \quad (12)$$

$$RP_{thighmale} = [6.64\ 7.18\ 7.18\ 1.33] \qquad RP_{thighfemale} = [6.48\ 7.49\ 7.30\ 1.24]$$

Elderly participants:[7]

$$COM_{thighmale} = HJC + (KJC - HJC) * 0.417 \qquad COM_{thighfemale} = KJC + (AJC - KJC) * 0.390 \quad (13)$$

$$m = 0.1032 * bodymass + 12.76 * L * C^2 - 1.023$$[12]

Abdomen

Note that for for the calculation of the anatomical coordinate system we assume the subject to be standing upright.

Markers	Calculation ACS
1. Right Anterior Iliac Spine (RASIS) 2. Left Anterior Iliac Spine (LASIS) 3. 8th thoracic vertebrae (T8) 4. Sternum xiphoid process (PX) MASIS = (RASIS+LASIS)/2 5. Additional marker (RPSIS) 6. Additional marker (LPSIS)	$x_{temp} = MASIS - T8$ z = [0 0 1] y = $x_{temp} \times z$ x = y $\times z$
Calculated joint centres	Segment length[5]
No joint centres calculated	$L = \lvert z_{navel} - z_{PX} \rvert * 1.035$ *Navel approximated from photos, see pelvis

Young participants:[5][8]

$$xy_{COM} = xy_{T8} + (xy_{PX} + xy_{navel})/2 - xy_{T8})) * 0.48_{[8]} \quad (14)$$

$$z_{COM} = z_{navel} + (z_{PX} - z_{navel}) * K_{a[5]}$$

Where $K_a = 0.5498$ for male, $K_a = 0.5488$ for female

$$RP_{abdomenmale} = [8.49\ 20.65\ 12.60\ 1.43] \qquad RP_{abdomenfemale} = [8.55\ 18.73\ 12.54\ 1.40]$$

Elderly participants:[7][13]

$$Vs(C0,D0,C1,D,h) = Vs(Cpelvis,D0,Cabdomen,D1,L) \quad (15)$$

$$D0 = ||xy_{MASIS} - xy_{T8}||\ D1$$

$$= ||xy_{T8} - xy_{PX}||\ w0 =$$

$$C_{pelvis},w1 = C\ m = (920 +$$

$$1010)/2 * Vs$$

For the COM location the same method was used as for young participants.

Upper arms

No adjustments were made to the models proposed by Leva[5] and Pavol[7].

Markers	Calculation ACS
1. Top lateral scapula marker (S1) 2. Lateral Humeral Epicondyle (LHE) 3. Medial Humeral Epicondyle (MHE) 4-7. Additional cluster markers (HU1-4)	$y_{temp} = MHE - LHE$ for right side $y_{temp} = LHE - MHE$ for left side z = SJC-EJC x = $y_{temp} \times z$ y = z $\times x$

Calculated joint centres	Segment length[5]
1. Shoulder Joint Centre (SJC) SJC = S1 + (EJC-S1)*0.108[5] 2. Elbow Joint Centre (EJC) EJC = (LHE + MHE) / 2	$L = \|\|SJC - EJC\|\| * 244.8/281.7$ for male $L = \|\|SJC - EJC\|\| * 235.9/275.1$ for female

Young participants:[5]

$$COM_{male} = SJC + (EJC - SJC) * 0.5772 \quad COM_{female} = SJC + (EJC - SJC) * 0.5754 \tag{16}$$

$$RP_{upperarmmale} = [9.67\ 10.81\ 9.71\ 2.06] \quad RP_{upperarmfemale} = [9.49\ 10.50\ 9.18\ 2.34]$$

Elderly participants:[7]

$$COM_{male} = SJC + (EJC - SJC) * 0.468 \quad COM_{female} = SJC + (EJC - SJC) * 0.479 \tag{17}$$

$$m = 0.0288 * bodymass$$

Thorax

The T12L1 joint is only calculated to structure the 3D plot. The segment length is determined by the location of the seventh cervical vertebrae (C7) and the xiphoid (PX).

Markers	Calculation ACS
1. Sternum xiphoid process (PX) 2. 8th thoracic vertebra (T8) 3. Sternum jugular notch (IJ) 4. 7th cervical vertebra (C7) 5. Right top scapula (RS1) for Pavol method 6. Left top scapula (LS1) for Pavol method 7. Right sternoclavicular joint (RSC) 8. Left sternoclavicular joint (LSC) 9. Sternum manubrium (MA)	$x_{temp} = (PX + IJ)/2 - (C7 + T8)/2$ z = [0 0 1] y = z $\times x_{temp}$ x = y $\times z$ Acromion = (RS1+LS1)/2 Shoulder = (RSJC+LSJC)/2
Calculated joint centres	Segment length
1. T12L1*to structure 3D plot T12L1 = C7 + gRseg*[0 0 -0.3] 2. RSJC from upper arm 3. LSJC from upper arm	L = abs(PX(3)-C7(3))

Young participants:

$$xy_{COM} = xy_{T8} + ((xy_{PX} + xy_{IJ})/2 - xy_{T8}) * 0.45^{[8]} \tag{18}$$

$z_{COM} = z_{PX} + (z_{C7} - z_{PX}) * K_t$ where $K_t = 0.4934$ for male, $K_t = 0.4950$ for female[5]

$$RP_{thoraxmale} = [5.72\ 21.83\ 9.35\ 1.35] \quad RP_{thoraxfemale} = [5.33\ 21.71\ 9.83\ 1.33]$$

Elderly participants with the three components as described in Pavol:[7][13]

$$m_{neck} = 1110 * (z_{C7} - zAcromion) * (C_{neck}^2/(4 * \pi) \tag{19}$$

$$m_{shoulder} = 1040 * \pi * w_{shoulder} * D_{shoulder} * (z_{Acromion} - z_{Shoulder})/4$$

where $w_{shoulder} = ||RS1 - LS1||$ and $D_{shoulder} = ||xy_{IJ} - xy_{C7}||$

$$m_{lowthorax} = 920 * Vs(C_{abdomen}, D0, C_{shoulder}, D1, L_{lowthorax}) \text{ where}$$

$$D0 = ||xy_{PX} - xy_{T8}|| \text{ and } D1 = ||xy_{IJ} - xy_{C7}||$$

$$C_{shoulder} = ||RS1 - LS1|| * \pi \text{actual width used in } V_s \text{ calculation}$$

$$L_{lowthorax} = z_{Shoulder} - z_{PX}\, m =$$

$$m_{neck} + m_{shoulder} + m_{lowthorax}$$

for the COM location same method as young participants was used

Lower arms and hands

The lower arm and hand together form one segment as the position of the hands is assumed to not have much influence on the estimation of the total body COM location.

Markers	Calculation ACS
1. Lateral Humeral Epicondyle (LHE) 2. Medial Humeral Epicondyle (MHE) 3. Radial Styloid (RS) 4. Ulnar Styloid (US) 5-8. Additional cluster markers (U1-4)	$y_{temp} = US - RS$ for right side $y_{temp} = US - RS$ for left side x = $y_{temp} \times z$ y = z $\times x$
Calculated joint centres	Segment length[5]
1. Elbow Joint Centre (EJC) EJC = (LHE+MHE)/2 2. Wrist Joint Centre (WJC) WJC = (US+RS)/2 3. 3th finger tip (FT3) FT3 = WJC+((WJC-EJC)/$L_{armstandard}$) *$dactilon_{standard}$	$L_{arm} = \|\|EJC - WJC\|\| * 251.3/268.9$ for male $L_{arm} = \|\|EJC - WJC\|\| * 247.1/264.3$ for female $L_{hand} = \|\|FT3 - WJC\|\| * 189.9/187.9$ for male $L_{hand} = \|\|FT3 - WJC\|\| * 172.0/170.1$ for female

Young participants:[5]

$$COM_{armmale} = EJC + (WJC - EJC) * 0.4574 \qquad COM_{armfemale} = EJC + (WJC - EJC) * 0.4559 \quad (20)$$

$$RP_{lowerarmmale} = [6.26\ 7.55\ 7.03\ 1.51] \qquad RP_{lowerarmfemale} = [6.43\ 7.81\ 7.95\ 1.14]$$

$$COM_{standard} = dactilon_{standard} * 0.3624$$

$$COM_{hand} = WJC + ((WJC - EJC)/L_{armstandard}) * COM_{standard}$$

$$RP_{handmale} = [5.54\ 6.65\ 4.86\ 2.29] \qquad RP_{handfemale} = [5.56\ 5.85\ 4.32\ 1.58]$$

where $dactilon_{standard} = 187.9$ for male and $dactilon_{standard} = 170.1$ for female, $L_{armstandard} = 268.9$ for male and $L_{armstandard} = 264.3$ for female Elderly participants:[7]

$$m_{arm} = 0.0169 * bodymass \quad m_{hand} = 0.0063 * bodymass \text{ for male} \qquad (21)$$

$$m_{arm} = 0.0135 * bodymass \quad m_{hand} = 0.0052 * bodymass \text{ for female}$$

$$COM_{armmale} = EJC + (WJC - EJC) * 0.430 \; COM_{armfemale} = EJC + (WJC - EJC) * 0.431 \; COM_{handmale} = WJC + L_hand * K_h \text{ where } K_h = 0.362 \text{ for male and } K_h = 0.343 \text{ for female}$$

For all participant groups combine both the lower arm and hand segment to one segment:

$$m = m_{arm} + m_{hand}$$

$$COM = (m_{arm} * COM_{arm} + m_{hand} * COM_{hand})/m$$

Head

The head's location is approximated extrapolating the spine indicated by the markers PX and T8 assuming a standard ratio between the height of the thorax and the length of the head. The assumptions holds if the head is in an upright position while in the calibration posture.

Markers	Calculation ACS
1. Sternum xiphoid process (PX) 2. 8th thoracic vertebra (T8) 3. Sternum jugulae notch (IJ) 4. 7th cervical vertebra (C7) 5. Right sternoclavicular joint (RSC) 6. Left sternoclavicular joint (LSC) 7. Sternum manubrium (MA)	$x_{temp} = (PX + IJ)/2 - (C7 + T8)/2$ z = [0 0 1] y = z $\times x_{temp}$ x = y $\times z$
Calculated joint centres	Segment length[5]
No joint centres calculated	$L = \lvert z_{C7} - z_{PX} \rvert * 249.9/242.1$ for male $L = \lvert z_{C7} - z_{PX} \rvert * 243.7/228.0$ for female *standard lengths from Zatsiorsky/Leva

$$COM = C7 + \frac{K_h * L/100 * (C7 - T8)}{|C7 - T8|} \qquad (22)$$

where $Kh = 0.4998$ for male and $Kh = 0.5159$ for female

Younger participants mass with Zatsiorksy/Leva parameters:[5]

$$RP_{headmale} = [6.37\ 8.68\ 9.38\ 1.25] \qquad RP_{headfemale} = [5.39\ 7.36\ 8.68\ 1.33]$$

Elderly participants mass:[7]

$$m = 14.6 * (height - z_{C7}) + 8.88 * C + 1.78 * C_{neck} + 19.9 * C/100/\pi - 7.385$$

Accuracy of the anthropomorphic model

The accuracy of the anthropomorphic model is determined with larger set of participants than used for the SB computation:

	N	MEAN AGE (SD) [Y]	MEAN BMI (SD)
YM	12	27.3 (4.3)	23.4 (2.7)
YF	14	27.1 (4.9)	22.6 (3.0)
EM	10	76.3 (7.0)	26.1 (3.7)
EF	12	75.0 (5.3)	25.2 (3.7)

Table 5 BMI data participant group

We assess the model by the performance factor:

$$Model\ Performance = \frac{\sum estimated\ segment\ mass}{total\ measured\ mass}\ [\%]$$

As the participants are clothed, and wear shoes, the model performs best if it slightly underestimates the total measured mass. In table 7 we see that for all categories except for the young women the estimated mass is larger than the measured mass.

	total	Young male (YM)	Young female (YF)	Elderly male (EM)	Elderly female (EF)
n	48	12	14	10	12
mean (SD) [%]		104.5 (4.6)	97.3 (4.7)	107.3 (7.8)	103.5 (4.7)

Table 6 Model performance mean and standard deviation per age-gender-group

The circumferences of the body segments have a large influence on the BSP estimation. BMI can account for approximately 50% of the BSPs[12] and so has a large influence on the total mass. Our set of participants is largely varied. The model performance per participant, dependened on BMI, is presented in figure 12. Previously reported model performance is approximated to be between 95% and 105% [13], indicated with a dashed line. There is no clear BMI influence indicating the BMI dependency on the circumference approximation is performed adequately.

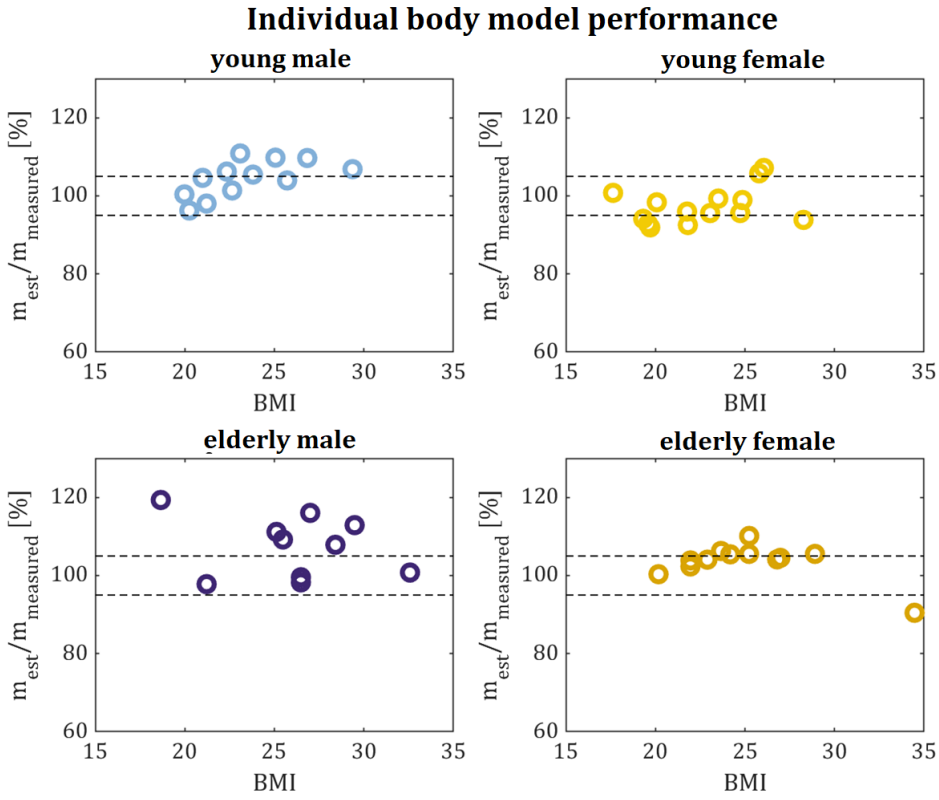

Figure 8 The participant's individual body model performance values per age-gender-group

Segment mass approximation result are varied. However, this is expected to be so as our participants are very different as well. To have an indication of the estimated mass per segment in kilo's we refer to table 8.

segment	est mean [kg]	est SD [kg]
foot	1.00	0.32
calf	2.92	0.91
thigh	8.71	3.81
pelvis	8.91	3.15
abdomen	8.63	4.16
thorax	14.13	4.73
upper am	1.86	0.57
lower arm	1.36	0.49
head	4.73	1.18

Table 8 Estimated masses of the body segments.

In figure 13 we have differentiated per category and compared the estimated masses to mean segment masses of a known data of a comparable subject group[14,15].

$$Segment\ Performance = \frac{estimated\ segment\ mass}{literature\ referential\ value\ (group)}\ [\%]$$

A large standard deviation within a subject group is accounted for by the variability of the subjects within the group. Large differences in mean values between the groups is accounted for by the model choice. For young participants the thigh and thorax are slightly overestimated whilst the abdomen is underestimated. Our choice of boundary between the two segments was lower than literature's 'usual application' thus this can be explained. The abdomen and thorax of the elderly group are larger than literature's referential values, this is due to our simplification of the Pavol model where we assume the circumference of the abdomen and thorax to be perfectly round rather than 'oval/part rectangular', this might also account for the general overestimation. These effect are expected to have a maximum of 5 cm effect on the height of the total body centre-of-mass.

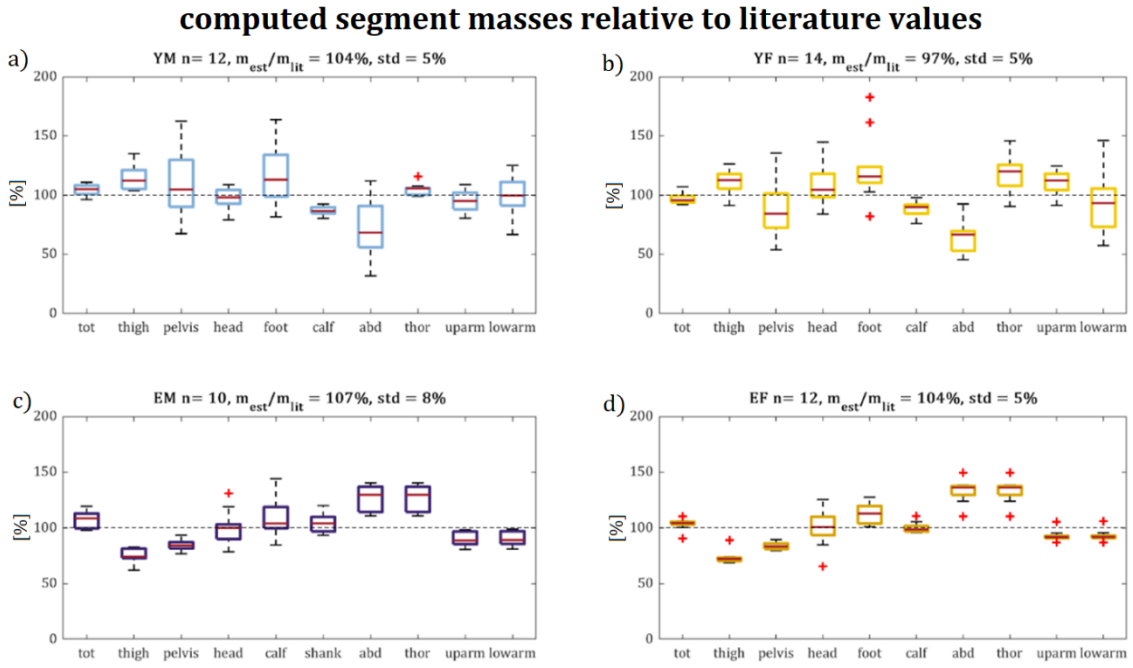

Figure 13 Segment performance (estimated mass / literature average mass) per participant group

C – Trial normalisation: detailed process

The average nominal trajectory is computed first. To do so the observed state trajectories (traj1, traj2, traj3) are aligned to the peak horizontal COM velocities. The average nominal trajectory ($traj_{avnom}$) is the average of the aligned state trajectories. (figure 14b) The $traj_{avnom}$ is cut to start at ($\tau = 0$) when the horizontal COM acceleration first exceeds 15% of its maximum. The $traj_{avnom}$ is cut to end ($\tau = T_{nom}$ when it first exceeds 99% of the maximum vertical COM position. The $traj_{avnom}$ is normalised by scaling the velocities with T_{nom} and to divide it's time vector τ_{avnom} by T_{nom} resulting in the normalised time vector t_{avnom}.

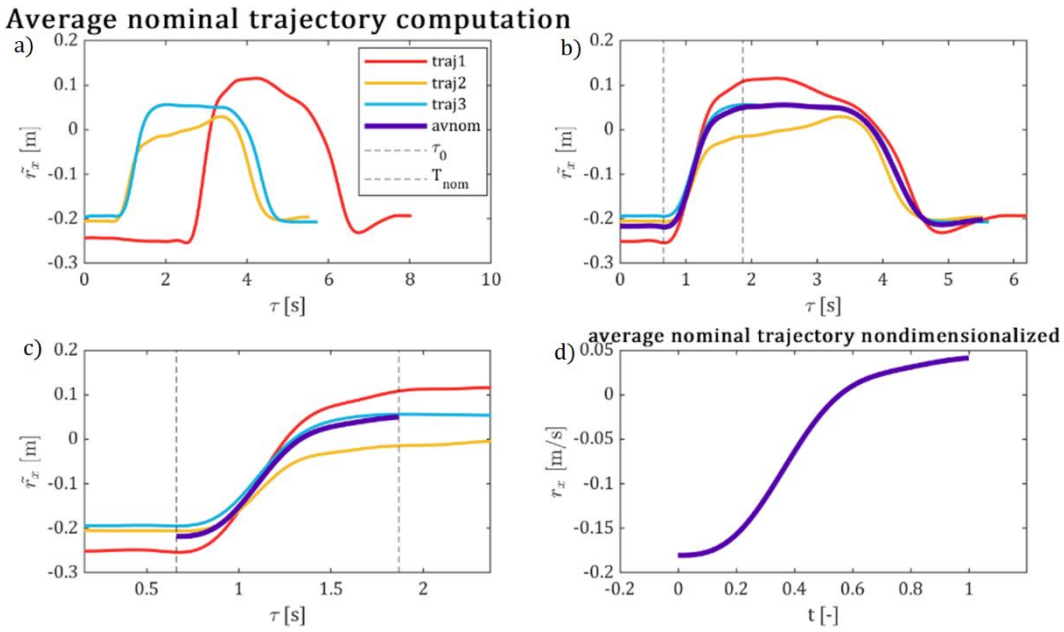

Figure 149 Trial normalisation: Average nominal trajectory computation

The iterative process to cut and align the observed state trajectories iterates over $T = [T_{min}, T_{max}]$ in 100 steps where $T_{min} = 0.75s$ and $T_{max} = 1.5*T_{nom}$. Each iteration $traj_{avnom}$ is scaled to run from 0 to T. Then we align and cut the measured state trajectory to the peak horizontal acceleration of $traj_{avnomscaledtoT}$ and the interval [0,T] to form $x_{segmentedtoT}$. We compute the root squared mean error (RSME) of $traj_{avnomscaledto}\}$ and $x_{segmentedtoT}$. We use $x_{segmentedtoT}$ where T has the smallest RSME from all iterations for normalisation.

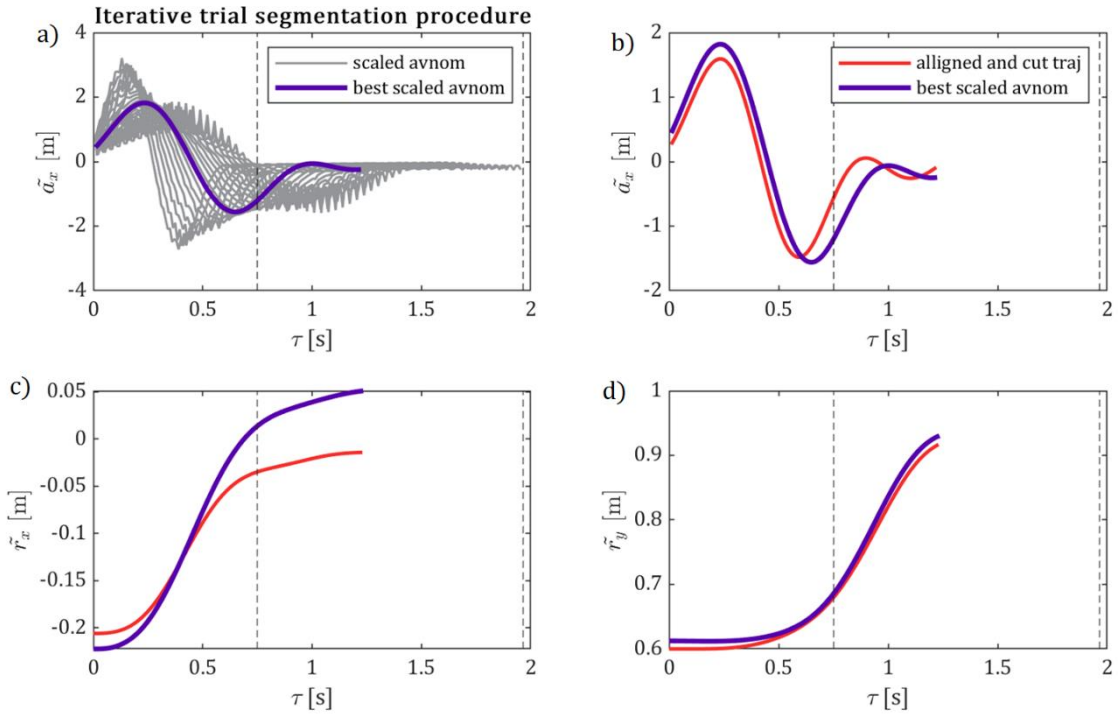

Figure 15 Trial normalisation: Iterative segmentation procedure

Each aligned and segmented state trajectory x(τ) is normalised. The time vector τ is divided over the trial's length T such that the unitless time interval t = [0,1][-], or 0 to 100% STS, is obtained. The state trajectory x(t) is normalised by scaling the velocity components with trial length T.

$$\tau = [0, T]\ [s] \rightarrow t = \frac{\tau}{T} = [0,1]\ [-]$$

$$\tilde{x}(\tau) = \left[\widetilde{r_x}(\tau)\ \ \widetilde{v_x}(\tau)\ \ \widetilde{r_y}(\tau)\ \ \widetilde{v_y}(\tau)\right]'$$

$$x(t) = [\widetilde{r_x}(T*t)\ \ T*\widetilde{v_x}(T*t)\ \ \widetilde{r_y}(T*t)\ \ T*\widetilde{v_y}(T*t)]'$$

$$x(t) = \left[r_x(t)\ \ v_x(t)\ \ r_y(t)\ \ v_y(t)\right]'$$

D - Parameter regression analysis

Performance parameter and age regression analysis results. The area of the target set and average time [s] of the three observations used as input for the stability basin have a significant positive relation to the stability basin size. A large target set area indicates less consistent end points and, we assume, strategy. A high mean value for t_{end} indicates slower sit-to-stand. The acceleration range is the mean difference between the maximum and minimum acceleration over the three trajectories. A smaller acceleration range indicates a more smooth sit-to-stand movement. The acceleration range has a stronger correlation to the stability basin of sit-to-stand without thigh push-off than to the stability basin of sit-to-stand with thigh push-off. Figure 17 presents the distribution of the minimum and maximum observed accelerations per arm-strategy.

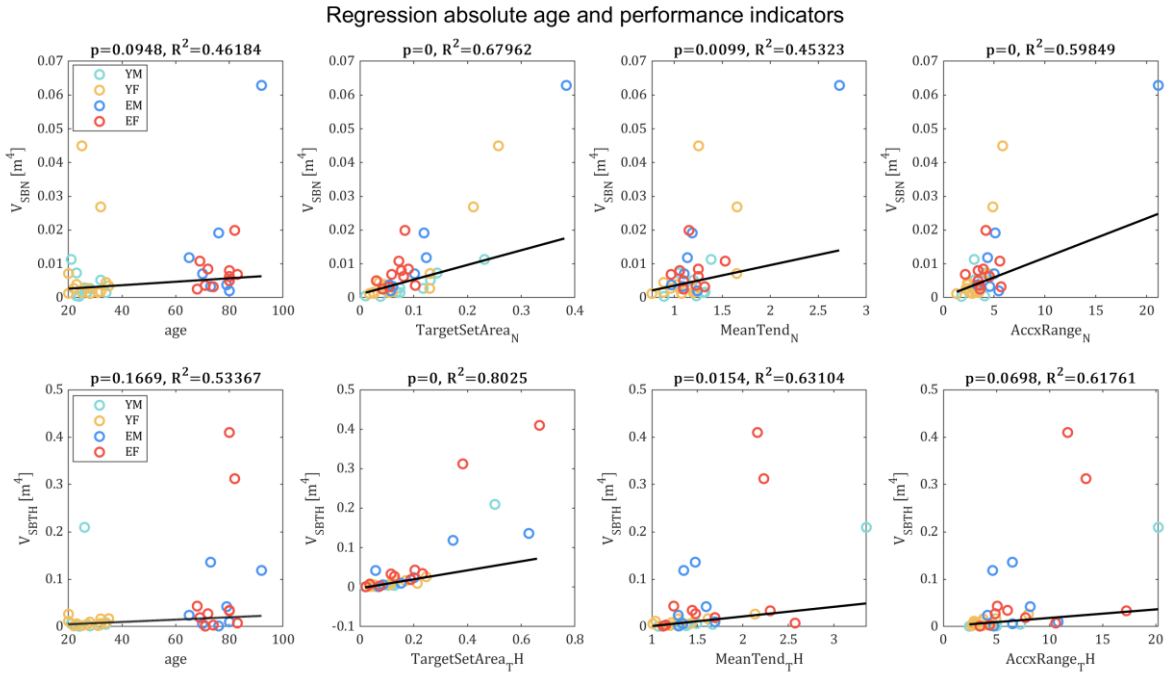

Figure 16 Regression analysis visualisation

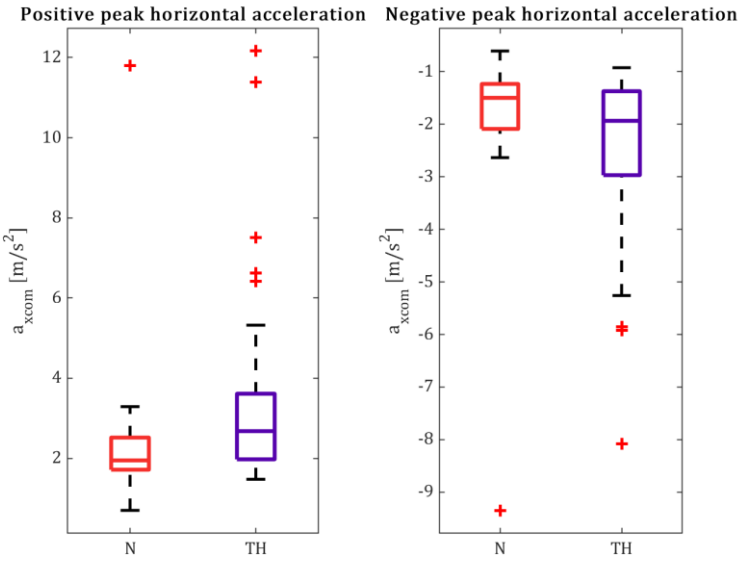

Figure 17 Observed acceleration range distribution per arm-strategy: No-arm (N) or thigh push-off (TH).

E – Controller model input check

In figure 18 we visualised the modelled input for an observed trajectory for three different controllers: LQR (optimised feedback), FFFB (using feedforward and feedback optimalisation) and BFFFB (input bound, feedforward and feedback optimalisation with a minimum and maximum computed input).[17] We compared the computed controller input with 'observed input'. The observed input, or direct input, is obtained directly from the observed trajectory from inverse dynamics using the equation of motion (*eq1*).

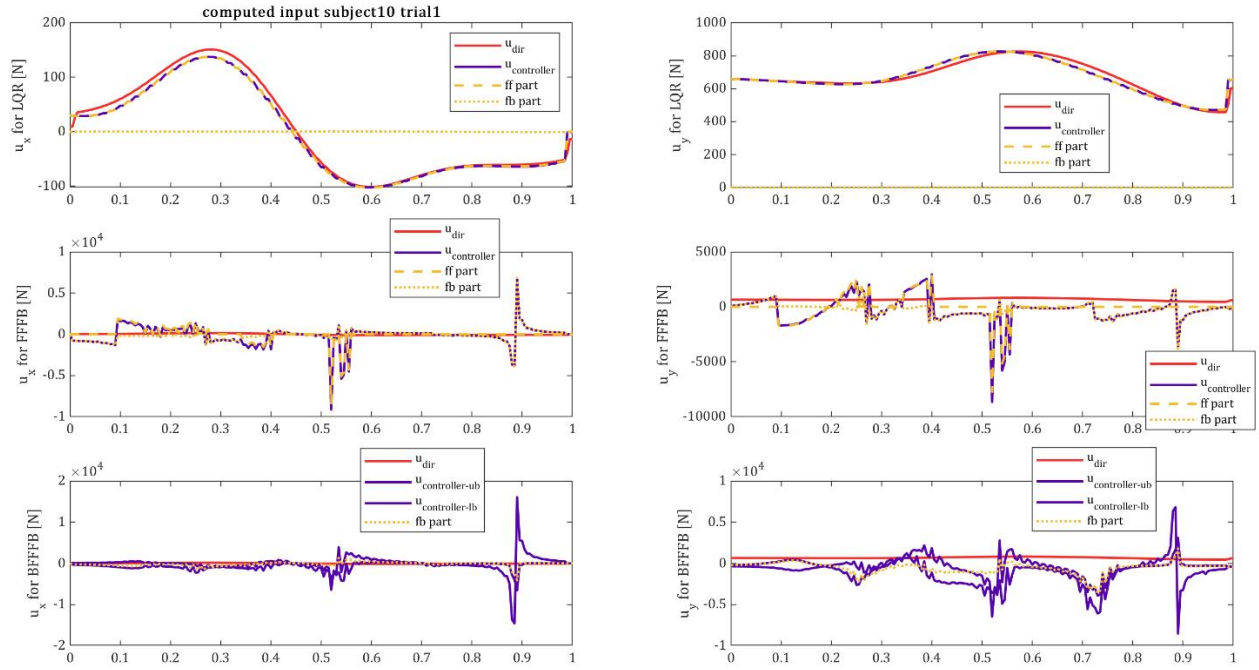

Figure 18 Controller model check: viualosation of controller ouptut u(t,x(t)) and observed input u_{dir} obtained from direct inverted dynamics.